General Disclaimer

One or more of the Following Statements may affect this Document

- This document has been reproduced from the best copy furnished by the organizational source. It is being released in the interest of making available as much information as possible.

- This document may contain data, which exceeds the sheet parameters. It was furnished in this condition by the organizational source and is the best copy available.

- This document may contain tone-on-tone or color graphs, charts and/or pictures, which have been reproduced in black and white.

- This document is paginated as submitted by the original source.

- Portions of this document are not fully legible due to the historical nature of some of the material. However, it is the best reproduction available from the original submission.

Produced by the NASA Center for Aerospace Information (CASI)

A Comparative Study of Measurements from Radiosondes, Rocketsondes, and Satellites

M. S. Nestler

A Comparative Study of Measurements from Radiosondes, Rocketsondes, and Satellites

M. S. Nestler

Department of Meteorology
The Pennsylvania State University
University Park, PA 16802

NASA

National Aeronautics and
Space Administration

Goddard Space Flight Center
Wallops Flight Facility
Wallops Island, Virginia 23337

ACKNOWLEDGMENTS

I extend my deepest appreciation to my thesis adviser, Professor John J. Olivero. This thesis could not have been completed without his steady stream of suggestions, encouragement, and good humor. In addition, during the course of my graduate study, he has shared with me his ideas and philosophy on not only meteorology, but on science in general. They are views which I will carry with me throughout my career in science.

I thank Professor Hans A. Panofsky for reviewing the thesis and for providing a number of useful comments which strengthened the final manuscript.

Thanks are also extended to Frank Schmidlin of NASA Wallops Flight Center for many helpful discussions on all aspects of this study.

This work was supported by NASA Wallops Flight Center under Contract No. NAS6-2726.

TABLE OF CONTENTS

LIST OF FIGURES

LIST OF TABLES

1.0 INTRODUCTION

An important goal of atmospheric research is to describe as completely as possible the structure of the atmosphere. The development of a variety of atmospheric measurement systems has contributed to progress toward this goal.

The first attempts to measure atmospheric temperature above the earth's surface occurred in the mid 1700's. Kites served as the platforms for these early temperature sensors (Middleton, 1969); routine flights of meteorological kites began about 1894. For the next thirty-five years, kites, along with captive and free balloons were used as platforms for the meteorgraph, an instrument designed to record readings from several meteorological instruments at once. Finally, the invention of the radiosonde by Molchanov in 1927 enabled temperature, pressure, humidity, and winds to be measured routinely in the troposphere. The book by Middleton (1969) gives a more detailed account of the evolution of instruments used to gather data above the earth's surface in the troposphere.

The gradual development of the radiosonde system, and particularly the development of higher quality carrier balloons, allowed the radiosonde to reach the lower stratosphere ($\sim$ 30 km maximum) during its ascent. The desire to study atmospheric structure above this level, however, provided the impetus for the use of rockets to propel sensors to great heights. The first attempt was made in 1946 with captured, German-built V-2 rockets. Further development of rockets followed a trend toward smaller, special-purpose devices. The Aerobee and Nike Cajun are examples of these types of systems. Today, the

meteorological rocketsonde (rocket and sensors) used in the United States is the Super Loki Datasonde. It provides temperature, pressure, and wind data at altitudes of 20 to 70 km for use in important areas of upper atmospheric research such as stratospheric warmings and the effects of stratospheric and mesospheric dynamics on the ozone distribution of the earth. For a detailed look at the development of rocketsonde systems, see Bollermann (1970).

It is important to note that shortcomings are present in the current radiosonde and rocketsonde networks. Too few soundings are made too far apart over limited areas to resolve adequately the great spatial and temporal variability of the atmosphere. For example, radiosondes are normally launched in the United States only every twelve hours at stations roughly 400 km apart. In addition, few launchings take place at sea. Lack of a sufficient number of measurements is an even greater problem at rocketsonde heights. Only about fourteen stations worldwide presently launch rocketsondes approximately once a week. It should be noted that there is even a possibility of a total cessation of rocket launchings (Schmidlin, personal communication). Unfortunately, factors such as economic considerations will probably allow the above shortcomings to continue.

A second problem with the in situ instruments is the disagreement among measurements taken by different instruments which are used by different countries. For example, Phillips et al. (1981) presented differences between the measurement capabilities of the NOAA, Vaisala, and Swiss radiosondes, while Finger et al. (1975) showed some incompatibility between rocketsondes used by the U.S., U.S.S.R., Japan, United Kingdom, and France.

A third difficulty with the _in situ_ devices is random and systematic errors. This point will be discussed later in this thesis.

The lack of a sufficient number of observations made globally in the troposphere and particularly in the stratosphere can be overcome with the increased use of operational satellite sounding systems. Satellite remote sounding has been an active area of research since the work of King (1956), who showed that the atmosphere's temperature profile could be determined from satellite measurements as a function of observation angle, and of Kaplan (1959), who showed that the temperature profile could be deduced from the spectral distribution of atmospheric emission. The first satellite measurement of atmospheric temperature was made from TIROS-7, which sensed emissions from the lower stratosphere (Kennedy and Nordberg, 1967). Later, NIMBUS-3 and NIMBUS-4 were used to determine temperature in seven layers of the troposphere and lower stratosphere (Wark and Hilleary, 1969). It was not until the early 1970's that a satellite (NOAA-2) was used to determine temperature for operational use (Jastrow and Halem, 1973). The development of the Pressure Modulator Radiometer (PMR) first flown on NIMBUS-6 allowed temperature observations to extend into the mesosphere (Curtis _et al._, 1974). Today, measurements from TIROS-N and its sister satellite NOAA-6 are used to determine mean temperatures in layers from the lower troposphere to the lower mesosphere. These temperatures are used operationally in stratospheric and mesospheric analyses of height fields, and in synoptic analyses of tropospheric height fields over oceans (Smith _et al._, 1979).

The ability of a satellite to provide a global network of more closely spaced soundings from the surface to the mesosphere is the

most important advantage it has over the _in situ_ instruments. In addition, since a single satellite makes the measurement, variability introduced with the use of different instrument types is eliminated. Unfortunately, disadvantages are also present. For example, a temperature measurement which is smoothed greatly in the horizontal and in the vertical can be a problem if finely-detailed atmospheric structure is desired. This and other difficulties and their implications is a major point to be discussed in this thesis.

Much remains to be done in the evaluation of operational satellite products used in conventional meteorological analyses. The identification and quantification of differences between satellite and _in situ_ systems can help to determine the optimal usage of satellite data in operational work or in research. The only way to address the above topic is to compare the measurements of the satellite to _in situ_ measurements assumed to be the "ground truth." Unfortunately, problems exist which can limit the usefulness of such comparisons. Usually, the two types of measurements are made at neither the same place nor at the same time. Each measurement also has different space and time scales; the satellite produces an instantaneous volume-averaged measurement while the _in situ_ instruments produce a series of point measurements which takes tens of minutes to complete. Finally, _in situ_ instrument errors can result in uncertainty about the "true" atmospheric structure.

The purpose of this study is to evaluate the comparability between large scale atmospheric structure (mean layer temperature, geopotential heights, and winds) determined from NOAA-6 and from radiosondes and rocketsondes. A major thrust is made to examine the impact of _in situ_ errors on satellite - _in situ_ comparability.

Chapter 2 describes the characteristics of each instrument (its method of measurement and sources of error). The _in situ_ instrument precision is detailed in Chapter 3. Chapter 4 discusses the satellite - _in situ_ statistical comparisons, while a summary of results and recommendations for future work are given in Chapter 5.

2.0   DESCRIPTION OF INSTRUMENTS

Before comparing in situ measurements and remote measurements, it is important to understand how each instrument senses large (synoptic) scale atmospheric structure and the accompanying errors involved. It should be noted at this point that the in situ error sources described in this chapter contribute mainly in a systematic fashion.

2.1   Radiosonde

2.1.1   Measurement Technique

This section briefly describes the function of a radiosonde. For a much more detailed description of this instrument, consult Wang (1975).

The standard NOAA radiosonde is a balloon-borne, battery-powered device used to determine a single vertical profile of pressure, temperature, geopotential height, mixing ratio, and wind in the troposphere and lower stratosphere ($\sim$ 30 km maximum). During its flight, the radiosonde is tracked with a Ground Meteorological Direction-finder (GMD-2) tracking system which consists of a small dish antenna telemetry receiver and a recorder. The radiosonde's position is found by tracking its 1680 MHz frequency-modulated signal with the antenna. The signals are also telecommunicated to the ground station where the recorder registers them in the form of traces on a paper strip chart. The traces must then be evaluated to obtain the meteorological data.

Temperature is determined electrically by a thin, white-coated rod thermistor. The thermistor is mounted unshielded from the sun on an outrigger outside the radiosonde and is connected to the radiosonde battery by lead wires. An electric current passed through the thermistor encounters increasing resistance as the thermistor temperature increases.

Humidity is measured electrically with a carbon-covered plastic strip known as a hygristor. This sensor is placed inside an air duct on the top of the radiosonde where it is shielded from precipitation and solar radiation. As the humidity increases, the strip expands which creates a change in its electrical resistance. Since the resistance of the strip is also temperature dependent, the thermistor temperature is also taken into consideration during the evaluation of the humidity data.

Pressure is determined with a temperature-compensated aneroid capsule. The capsule is connected by a contact arm to series of silver contact strips and insulating segments called a commutator. As the atmospheric pressure decreases, the aneroid capsule expands and moves the arm and a pointer across the commutator. This causes a change in the frequency of the transmitted signal; the temperature signal is transmitted when the pointer touches an insulating segment and the humidity signal is transmitted when the pointer touches a silver strip. A specific value of pressure is defined each time the signal frequency changes denoting a new contact. Each contact is numbered and a calibration chart is used to relate the contact number to the atmospheric pressure.

The geopotential height is a quantity calculated via the hypsometric equation

$$\Delta h = R \, \overline{T}_v \, \ell n \, \frac{P_0}{P_1} / g_o \qquad\qquad (2.1)$$

where Δh is the thickness of a layer bounded at the bottom by
pressure P_0 and at the top by pressure P_1, R is the dry gas constant
(287 j kg^{-1} K^{-1}), g_o is 9.8 ms^{-2}, and $\overline{T}_v$ is the mean virtual
temperature in that layer. The thicknesses are summed to give
the geopotential height of the radiosonde at pressure P_1.

The radiosonde is usually tracked either automatically with a
GMD or manually with a theodolite. Either instrument finds the
azimuth and elevation angles of the radiosonde during its ascent.
These angles are used along with the calculated heights to determine
the displacement of the radiosonde in a certain time, thus allowing
for the calculation of horizontal winds.

2.1.2 Sources of Error

A variety of sources can cause the temperature measurement to
be in error. Incorrect calibration before the flight (baseline
check) gives a systematic error throughout the entire flight. Lag
errors, due to the inability of the rod thermistor to detect rapidly-
varying temperatures, were found by Badgely (1975) to reach 0.3°C.
He considered this value to be unimportant, however. Ballard and
Rubio (1968) applied the heat transfer equation to study the effects
on the thermistor temperature of aerodynamic heating, conduction of
heat through the lead wires, and solar radiation. They found heating
from lead wire conduction to be small. Aerodynamic heating was
considered negligible because of the slow rise rate of the radiosonde
(~ 5 ms^{-1}). The most significant influence was from solar radiation.
Temperature corrections necessary to compensate for this influence

ranged from 0.5°C at 10 km to 2.0°C at 30 km. Later, McInturff et al.
(1979) examined day-night temperature differences from a large
sample of radiosondes and concluded that the NOAA radiosonde
temperatures should be corrected for solar radiation. Their
corrections, based on altitude, solar elevation angle, and
observation time agree with the results of Ballard and Rubio. It
must be noted here, however, that no corrections are applied to
current operationally-used radiosonde temperature data nor were they
used in the observations to be reported in this study.

Solar radiation also tends to affect the humidity measurements.
Even though the hygristor is mounted in a way which shields it from
the sun, Finger and McInturff (1978) have noted some error at high
solar elevation angles.

Pressure is also subject to a number of errors. Improper base-
line calibration introduces systematic errors. There is the
possibility of air leaking into the aneroid cell. This would cause
faulty cell expansion and an incorrect pressure measurement. A
third factor is wear on the contacts themselves, which could cause
the pointer to move irregularly over the contacts.

All the above error sources influence the computed geopotential
height. Errors in pressure and temperature propagate through the
hypsometric equation to affect directly the geopotential height
calculation. These effects will be examined in Chapter 3. Since
mean virtual temperature is used in the hypsometric equation,
humidity errors can also contribute somewhat to geopotential height
errors. This contribution is relatively small in comparison with
height errors associated with errors in the kinetic temperature
measured by the rod thermistor.

Errors in the tracking of the radiosonde by the GMD (i.e. errors in the azimuth and elevation angle) along with errors in the calculated height of the radiosonde lead to erroneous wind data. It is beyond the scope of this thesis to examine errors in the GMD and their effect on wind calculations; please consult Danielsen and Duquet (1967) for a discussion of these topics.

2.2 Meteorological Rocketsonde

2.2.1 Measurement Technique

The meteorological rocketsonde used in this study is the Super Loki Datasonde. This instrument provides direct determination of temperature and wind as a function of geometric altitude to approximately 70 km. It is comprised of four principal components: the Super Loki booster rocket, the datasonde dart, the datasonde (which contains the temperature sensor), and the Starute (Stabilization and Retardation Parachute), which is a reflective decelerator. The rest of this section describes the rocketsonde system and how it makes measurements; for a comprehensive discussion of rocketsonde systems, see Bollermann (1970).

A rocketsonde flight is summarized in Figure 2.1, taken from Krumins (1976). The Super Loki rocket delivers the dart containing the datasonde and Starute to the burnout altitude. There, the dart separates from the rocket and continues upward until apogee ($\sim$ 70-80 km) is reached. At apogee, the datasonde and Starute are deployed and begin to descend (Figure 2.2). During descent, the datasonde transmits its temperature data to a ground-based GMD. At the same
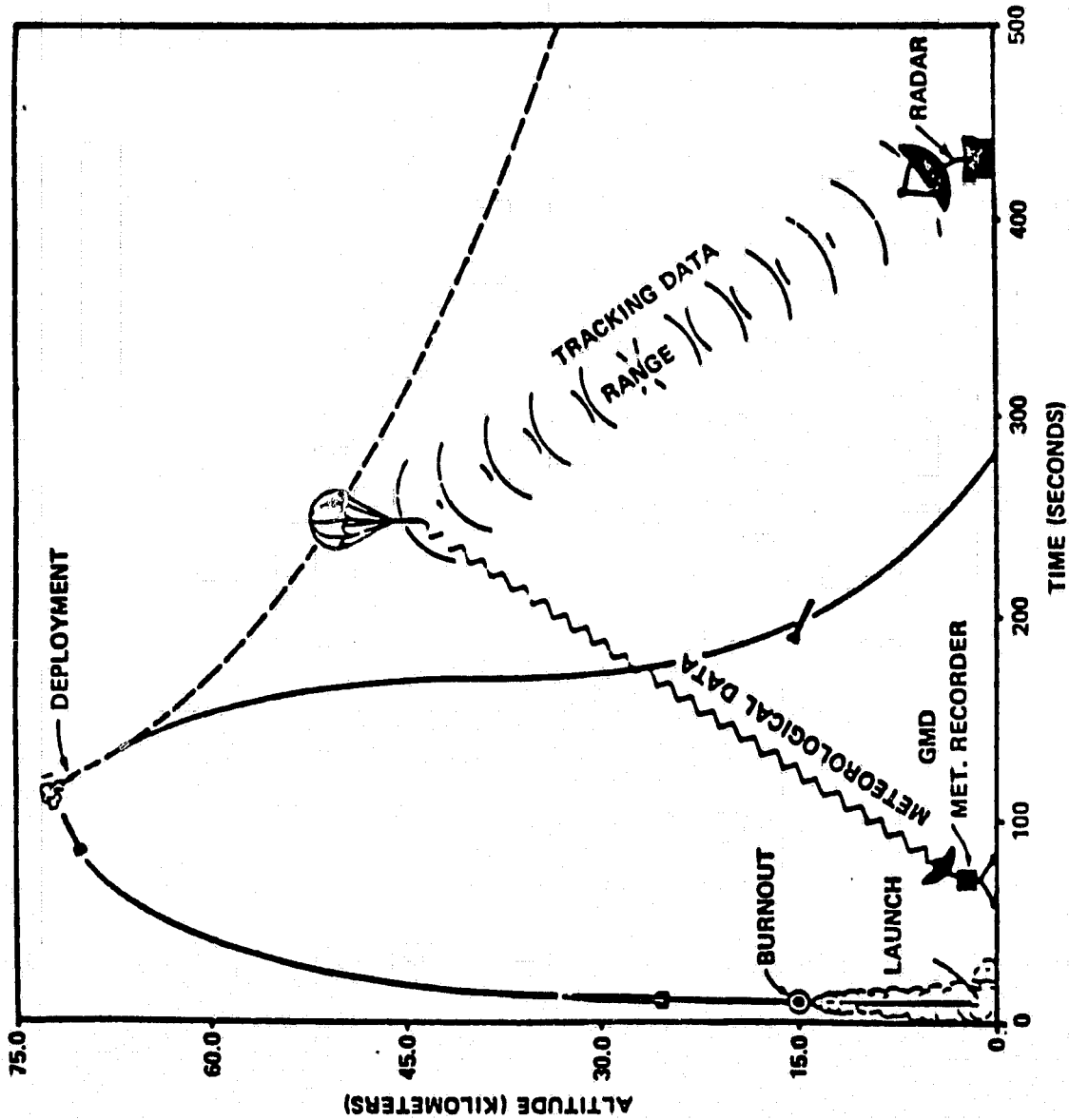
Figure 2.1 Typical rocketsonde flight (from Krumins, 1976).
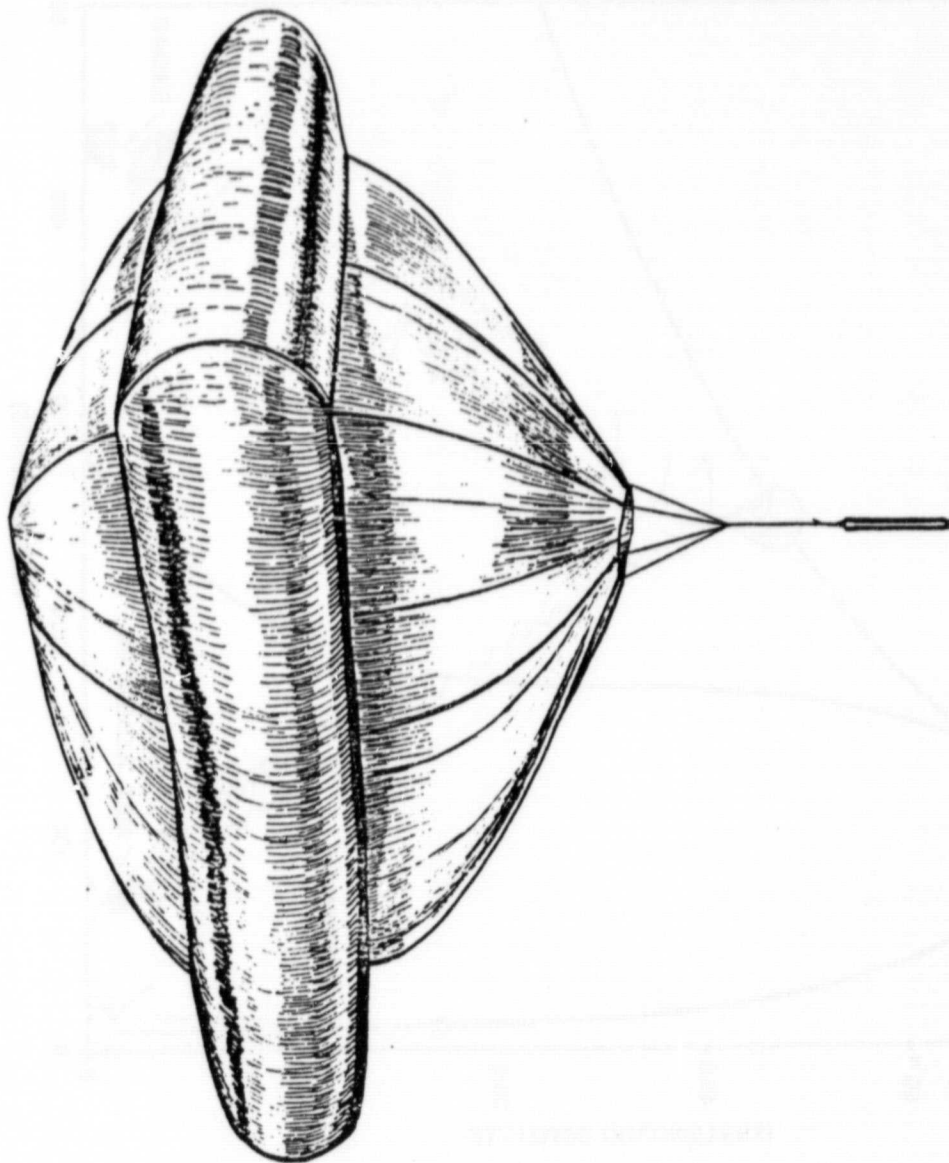
Figure 2.2 Sketch of the datasonde and the decelerator (from Krumins, 1976).

time, a precision radar tracks the Starute to obtain a time-position plot of the datasonde.

Temperature is determined with a 10-mil diameter bead thermistor. The small bead has a much faster response time than a rod thermistor; this is necessary at high altitudes because of the high fall velocity of the datasonde, the diminished molecular collision frequency, and lowered heat transfer rates. Figure 2.3, again from Krumins, shows the location of the bead thermistor and its mount at the base of the datasonde. The thermistor is mounted on a flexible loop of thin mylar film. The loop protects the thermistor from the shock of launch and is resilient to endure the strains of the datasonde separation from the dart. The inside of the loop is covered with a reflective aluminum coating to shield the thermistor from infrared radiation from the datasonde itself. Two silver strips run along the outside of the loop and serve as a path for an electric current from the thermistor to the lead wires. This current originates from the datasonde battery and is used, as with the rod thermistor, to measure changes in thermistor resistance as the temperature changes.

The radar tracking of the Starute enables horizontal winds to be obtained. The position of the descending datasonde as a function of time is calculated using the slant range, elevation angle, and azimuth angle determined by the radar. The time dependence of the positional differences is used to calculate winds.

Unlike the radiosonde, the datasonde does not measure pressure. Instead, pressure is calculated assuming hydrostatic equilibrium with the excellent approximation
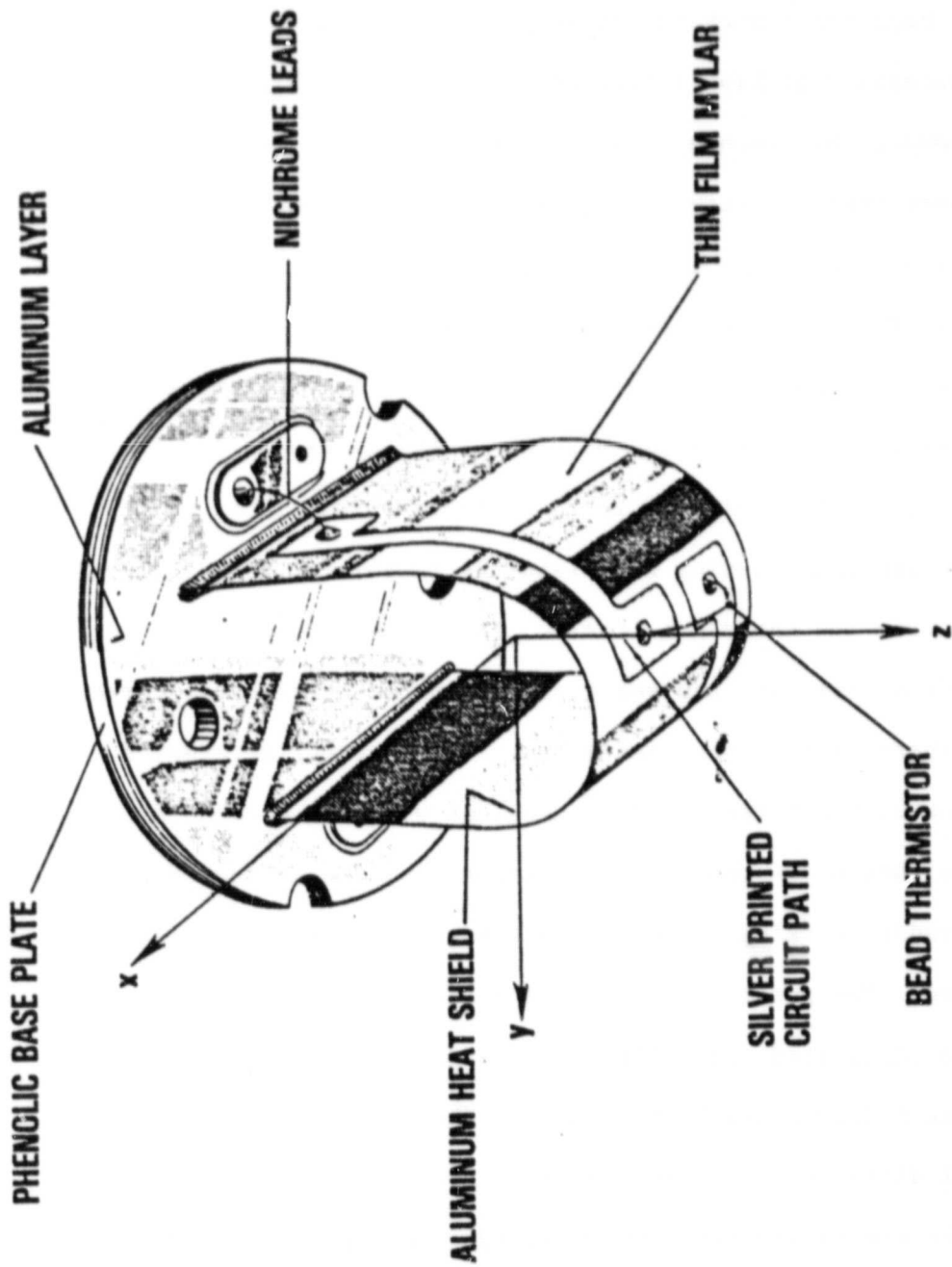
Figure 2.3 Sketch of the bead thermistor and its loop mount (from Krumins, 1976).

$$P_n = P_o \exp \left[- \sum_{i=1}^{n} \frac{g_o \, \Delta z}{R \bar{T}_{vi}} \right] \qquad (2.2)$$

where Δz is the layer thickness (usually 1 km), P_o is a "tie-on" pressure, and the other variables are as before. The tie-on pressure is particularly important. It is obtained from a support radiosonde launched near the time of rocket launch. A tie-on point (usually 20-25 km) is determined where the temperature-height profiles of the radiosonde and rocketsonde show the best overlap. The radiosonde pressure at that point is used for the tie-on pressure and Equation 2.2 is applied to calculate the pressure profile.

2.2.2 Sources of Error

The measure of temperature at very high altitudes is much more difficult than at lower altitudes. At very low densities, the fewer molecular collisions that take place result in less conduction of heat between the air and the bead thermistor. The decreased conduction increases the relative influence on the bead thermistor of heat sources other than accommodation with the air. These sources, most of which were relatively unimportant in the denser lower atmosphere, now contribute a large part of the total heat transferred into the bead thermistor. The actual air temperature is therefore masked. Aerodynamic heating is a major concern since the fall velocity of the datasonde can reach 200 ms^{-1} at 70 km before the Starute can effectively decelerate the payload. Direct or reflected solar radiation can influence the thermistor temperature since it is difficult to shade the bead totally. Exchange of longwave

(infrared) radiation with the instrument, atmosphere, and the earth's surface can affect the thermistor temperature. The electric current used to measure thermistor resistance heats the lead wires which in turn heat the thermistor via conduction. The current also heats the thermistor directly by encountering the resistance offered by the thermistor. The silver strips introduce yet another source of extraneous heating since they provide conduction paths for heat flow from the datasonde body to the lead wires and the thermistor.

In addition to extraneous heat sources, the bead thermistor temperature can be affected by time lag errors (as described for the radiosonde rod thermistor) and by initial temperature offsets. The latter effect results when the datasonde is ejected from the dart. The thermistor temperature usually starts out much greater than the atmospheric temperature until the thermistor comes substantially into equilibrium with the ambient atmosphere.

The determination of the air temperature from the bead temperature involves the application of correction factors derived from a mathematical model of the heat transfer into and out of the bead thermistor. The standard correction method is that designed by Krumins (1976), who analyzed the heat transfer equation to generate correction coefficients. The corrections range from approximately 2°C at 40 km to 8°C at 60 km, and become very large and unreliable at 70 km and above. Therefore, temperature measurements above 70 km are not attempted with the current rocketsonde system.

Since the altitude of the rocketsonde is determined from radar tracking, height errors can be caused by such things as the incorrect alignment of the datasonde with radar, electronic noise, and atmos-

pheric refractive index effects. The last item results in the slight bending of the radio waves to and from the radar, and if not corrected, causes the radar to "see" the Starute at an incorrect altitude. High precision FPS-16 tracking radars nevertheless have only small height errors of order 10 m (Engler et al., 1967).

Errors in rocketsonde winds result from errors in the slant range, azimuth angle, and elevation angle as determined by radar. Please see Luers and MacArthur (1971) for an analysis of wind errors incurred through radar tracking of descending sensors.

The calculation of the pressure profile with Equation 2.2 can be affected by errors in both the rocketsonde and its support radiosonde. Errors in radiosonde temperature and pressure lead to an incorrect pressure-height relationship, which in the overlap region results in an incorrect tie-on pressure. Errors in the rocketsonde temperature and height, along with the radiosonde errors, produce temperature-height profiles for each instrument that are very dissimilar to one another. This creates a problem in the determination of profile overlap and in the subsequent choice of the tie-on pressure. Figure 2.4 shows temperature profiles from a rocketsonde and radiosonde launched about one hour apart. Note the discrepancies between the two profiles in the overlap region. The tie-on problem is an important question, but there has been no published work on this subject. This problem is beyond the scope of this study, but certainly more investigation into the problem is needed.

2.3 NOAA-6 Satellite

This section describes some of the more important characteristics of the NOAA-6 polar orbiting satellite. Specifically, the NOAA-6
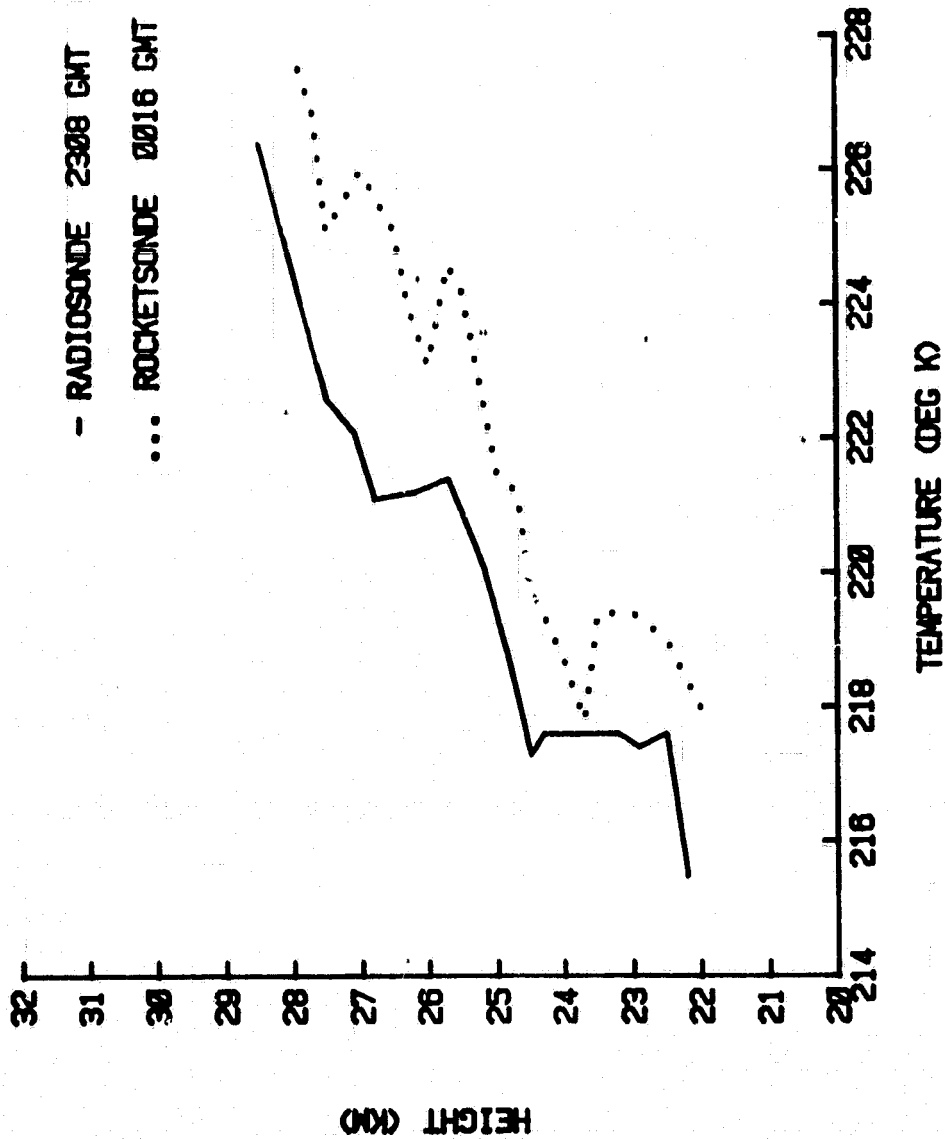
Figure 2.4 Temperature profile of a radiosonde and of a rocketsonde in the overlap region.

radiometers and their channels, the channels' weighting functions, and the techniques used to determine atmospheric temperature are examined. For a more detailed discussion of these topics, as well as a more extensive look at NOAA-6 in general, please see Schwalb (1978) and Smith et al. (1979).

2.3.1 Radiometers

There are three radiometer systems aboard NOAA-6: the second version of the High Resolution Infrared Sounder (HIRS-2), the Microwave Sounding Unit (MSU), and the Stratospheric Sounding Unit (SSU). These instruments are known collectively as the TIROS-N Operational Vertical Sounder (TOVS). This array of radiometers measures radiation emitted at many different wavelengths arising from different parts of the atmosphere. This measured radiation is used to determine the layer mean temperature for a number of standard pressure intervals.

HIRS-2 has twenty channels sensitive to infrared radiation emitted in the 3.7 μm and 15 μm regions by CO_2, H_2O, and N_2O. Table 2.1 summarizes the characteristics of the HIRS-2 channels. Radiation is sensed in circular fields of view (FOV) at the sub-satellite point and in elliptical FOVs as the radiometer scans away from the sub-satellite point. A cross-track scan of 2240 km forms fifty-six FOVs.

The four channels of the MSU are used to sense microwave emissions by the earth's surface and by O_2. Clouds are rather transparent to these emissions, a characteristic which, as will be discussed later, is useful when temperature soundings are deduced during cloudy conditions. Table 2.2 describes the characteristics

Table 2.1 Characteristics of HIRS-2 channels

HIRS Channel Number	Central Wavelength (μm)	Principal Absorbing Constituents	Level of Peak Energy Contribution	Purpose of Radiance Observation
1	15.00	CO_2	30 mb	
2	14.70	CO_2	60 mb	
3	14.50	CO_2	100 mb	
4	14.20	CO_2	400 mb	Atmospheric temperature sounding
5	14.00	CO_2	600 mb	
6	13.70	CO_2/H_2O	800 mb	
7	13.40	CO_2/H_2O	900 mb	
8	11.10	Window	Surface	Surface temperature and cloud detection
9	9.70	O_2	25 mb	Total ozone concentration
10	8.30	H_2O	900 mb	
11	7.30	H_2O	700 mb	Water vapor sounding
12	6.70	H_2O	500 mb	
13	4.57	N_2O	1000 mb	
14	4.52	N_2O	950 mb	
15	4.46	CO_2/N_2O	700 mb	Atmospheric temperature sounding
16	4.40	CO_2/N_2O	400 mb	
17	4.24	CO_2	5 mb	
18	4.00	Window	Surface	Surface temperature
19	3.70	Window	Surface	
20	0.70	Window	Cloud	Cloud detection

Table 2.2 Characteristics of MSU channels.

MSU Channel Number	Frequency (GHz)	Wavelength (mm)	Principal Absorbing Constituents	Level of Peak Energy Contribution	Purpose of Radiance Observation
1	50.31	5.96	Window	Surface	Surface emissivity and cloud attenuation
2	53.73	5.58	O_2	700 mb	Atmospheric temperature sounding
3	54.96	5.45	O_2	300 mb	
4	57.95	5.17	O_2	90 mb	

of the MSU channels. A single scan of the MSU produces eleven FOVs

along the same cross-track extent as that of HIRS-2. The horizontal

resolution is therefore much less than that of HIRS-2.

The three SSU channels, sensitive to 15 μm radiation emitted

by CO_2, enable temperature to be deduced at upper stratospheric and

lower mesospheric levels. Table 2.3 provides a summary of the SSU

channel characteristics. The SSU forms only eight FOVs along a scan

line of 1470 km. Smith et al. (1979) describe the data processing

used to interpolate the SSU FOVs, as well as the MSU FOVs, to each

HIRS-2 FOV. The result is a radiance sounding that consists of a

HIRS-2 measurement plus interpolated radiances from the MSU and the

SSU.

2.3.2 Weighting Functions

To deduce a vertical temperature profile from infrared and

microwave emission measurements, it must first be determined from

which areas of the atmosphere the measured radiation is being

emitted. The curves shown in Figure 2.5 are the weighting functions

for the TOVS channels. They show which layer of the atmosphere

contributes most to the total radiation sensed by a particular channel.

The total emission sensed by each channel can be used with each

weighting function to deduce a vertical temperature profile.

The weighting functions also illustrate a major shortcoming

of the satellite: the vertical smoothing of temperature. Consider

the shape of the HIRS-2 channel 3 weighting function. The function

peaks at 100 mb, but notice that it attains values of 0.2 or greater

in a layer from 500 mb to 10 mb. Therefore, infrared emission from

a large part of the atmosphere contributes to the total radiation

Table 2.3 Characteristics of SSU channels.

SSU Channel Number	Wavelength (μm)	Principal Absorbing Constituents	Level of Peak Energy Contribution	Purpose of Radiance Observation
1	15.0	CO_2	15.0 mb	Atmospheric temperature sounding
2	15.0	CO_2	4.0 mb	
3	15.0	CO_2	1.5 mb	
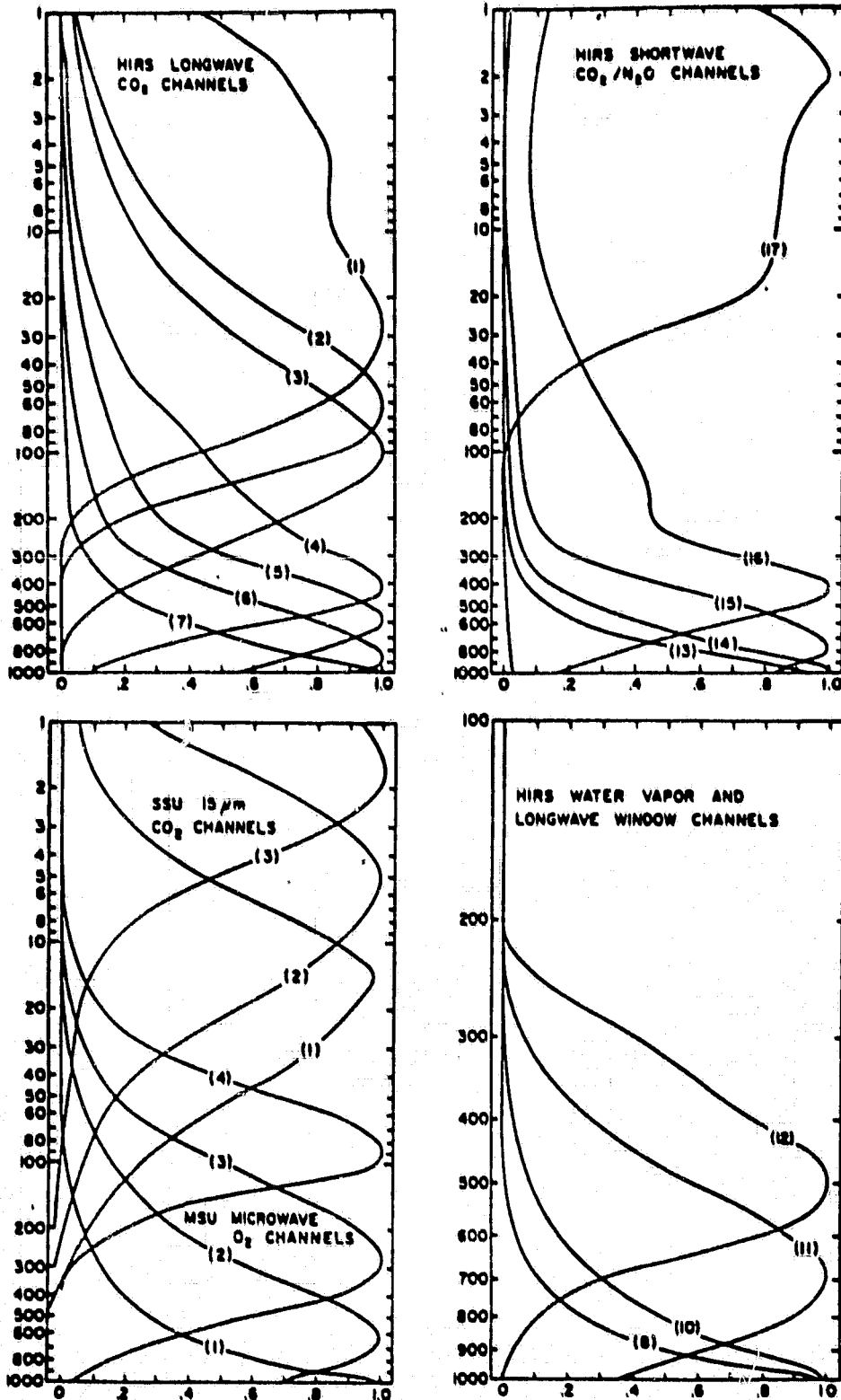
Figure 2.5   Normalized TOVS weighting functions.

sensed by channel 3. Similar arguments can be made for the other
twenty-six channels. The final result is that the determination of
temperature at a particular level will be influenced by emission
(and thus temperature) at other levels as well. The temperature
profiles deduced from the satellite measurements are vertically
smoothed profiles because of the width of the TOVS weighting functions.

2.3.3 Retrieval Methods

Clouds are opaque at the infrared wavelengths sensed by HIRS-2.
The measured radiances will be less than what is actually emitted
from the atmosphere if corrections for the presence of clouds are not
applied. Sets of sixty-three FOVs are formed and tested for cloudiness.
If enough FOVs are judged to be clear, radiances from all HIRS-2 and
MSU channels are used to form a volume-averaged sounding of the
thermal emission of the atmosphere; each sounding is separated by
250 km. Temperature soundings are determined statistically with
regression methods that employ radiance soundings from the satellite
which are colocated with radiosonde or rocketsonde temperature
soundings (Phillips et al., 1979).

If the sets are determined to be partly cloudy, clear radiances
are deduced statistically from the partially cloud-covered FOVs by
the N* technique, based on the method of Smith and Woolf (1976).
All channels are used in this technique. Should the atmosphere be
cloudy enough so that neither the clear nor N* methods is applicable,
the radiance value for each FOV set is a spatial average of radiances
from the four MSU channels and HIRS-2 channels 1, 2, 3, and 17.
These channels are assumed to be unaffected by clouds, although they
are affected by precipitation (Phillips, 1980). It should be noted

that although the retrievals are adjusted for clouds, clouds still pose a major obstacle to the accuracy of satellite data. For example, the cloud tests can only roughly approximate the cloudiness. Also, the cloudy retrieval is subject to large inaccuracies because only four channels of the twenty-seven available are used. Chapter 4 will elaborate further on these points.

2.4 Summary of Characteristics of In Situ and Satellite Measurements

The following characteristics of in situ and satellite measurements are noteworthy:

1. The current radiosonde network provides a limited number of observations over oceans and the polar regions. Over land, typical sounding separations average 400 km. The rocketsonde network provides even less coverage with about fourteen stations worldwide. The result is inadequate spatial resolution of the atmosphere.

2. The satellite provides full global coverage of soundings with a better spatial resolution (250 km).

3. The variety of in situ instruments used by different countries introduces additional variability into in situ measurements. This type of variability is not present in satellite data since a single instrument makes every measurement.

4. The radiosonde and rocketsonde provide point measurements, i.e. data taken along a unique path. This measurement is capable of "seeing" great detail in the vertical. The satellite measurement is a volume average smoothed

vertically and horizontally. It is not capable of
capturing great vertical or horizontal detail, although
combining the radiances from different channels does yield
better resolution.

5. Major error sources for each instrument include:

    a. satellite: cloud contamination of the infrared
        channels.

    b. radiosonde: extraneous heat sources, faulty
        aneroid cell.

    c. rocketsonde: extraneous heat sources, determination
        of tie-on pressure.

3.0   PRECISION OF IN SITU MEASUREMENTS

The reliability of the in situ measurements is
an important aspect of satellite-in situ comparisons. If the standard
to which satellite data are to be compared is not consistent in its
detail of atmospheric structure, it will be difficult to define the
"true" atmospheric conditions at the time of satellite overpass.
Moreover, it will then be difficult to evaluate how well the satellite
reproduces the "true" atmospheric structure. It must therefore be
determined how precisely the in situ measurements can characterize
the atmosphere.

3.1   Experiment Design

This study does not attempt to address the absolute accuracy of
the in situ sensors. Rather, we seek here the precision of the
in situ measurements. How repeatable are those measurements?

Precision is defined as the amount of agreement between measure-
ments taken from identical instruments at the same place and at the
same time. It is calculated by finding the root-mean-square difference
(rmsd) between paired measurements,

$$\sigma = \left(\sum_{i=1}^{N} (A_1 - A_2)_i^2 / N \right)^{1/2} \tag{3.1}$$

where σ is the rmsd and A_1 and A_2 are parameters measured by the
first and second instruments, respectively. The summation is taken
over all N differences at a particular level. The statistic says

nothing about the accuracy of an instrument; it does quantify the performance of two instruments relative to each other.

To evaluate the precision of radiosonde data, a special series of twenty-one dual radiosondes (two radiosondes hung from a single balloon) was flown from Wallops Island, Virginia from February 1980 to March 1981. The use of dual radiosondes eliminates space and time variability between measurements, and taking differences removes the true value of the parameter from consideration. The instrument variability should then be isolated (Grubbs, 1948). Three flights each lost one of the two radiosondes; the remaining eighteen pairs were used for the study of precision. Each radiosonde was hung 30 m below the balloon and separated from its partner by 2 m. With this configuration, it can be assumed that the instruments were sampling identical atmospheric conditions. Raw data recorded on the strip charts were carefully reduced by hand and processed by computer to give temperature, pressure, and geopotential height information at one-minute intervals. It is thought that these soundings are subject to less human error than a typical operational sounding. The precision of thermodynamic parameters was of interest in this portion of the study, so winds were not computed from the dual radiosonde data. Additionally, each flight was tracked by a precision C-band (FPS-16) radar to provide an independent means of altitude determination. The geometric altitude from the radar was converted to geopotential height with the relation (Iribarne and Godson, 1973):

$$h = \frac{9.8061}{9.8066} (1 - 2.59 \times 10^{-3} \cos 2\phi)z(1 - 1.57 \times 10^{-7}z) \qquad (3.2)$$

where h is the geopotential height, z is the geometric height, and
φ is the latitude. These radar geopotential heights will be compared
to geopotential heights calculated with the hypsometric equation.

For the study of rocketsonde precision, three rocketsondes were
launched at five-minute intervals from Wallops Island on ten NOAA-6
satellite overpass dates from February 1980 to May 1980. Temperature,
pressure, and wind data at 1 km intervals were evaluated for fifteen
successful measurement pairs. Rocketsondes launched five minutes
apart constituted a pair. Thus, for three launches on a given date,
flights one and two and flights two and three were considered to be
pairs. The rocket data, therefore, contain atmospheric temporal
and spatial variability as well as measurement error. The spatial
variability is introduced because, as Schmidlin (1981) found, rocket-
sondes launched on the same flight path could still be separated by
a constant distance of up to 10-12 km. Schmidlin also noted that
the ideal method for examining rocketsonde precision would be to
launch two or more datasondes on a single rocket (analogous to dual
radiosonde flights) but engineering problems, aerodynamic effects,
safety concerns, and cost make this technique difficult.

3.2 Radiosonde Precision

The usual purpose of the radiosonde is to assign temperature
and a calculated geopotential height to a measured constant pressure
surface. The "absolute" height, or the actual height of the radio-
sonde above the surface is not considered. This synoptic use of
the data results in the constant pressure charts familiar to all
meteorologists. It must be realized, however, that the radiosonde

is also used as an absolute reference for pressure or altitude.
For example, in the determination of vertical profiles of ozone,
the only way to locate the point where the ozone is being measured
is to use the instantaneous pressure and height as determined from a
single, attached radiosonde (Godson, 1963). It will be shown in
this section that radiosonde data used for synoptic purposes has high
precision, but the precision is reduced when the data are evaluated
as a function of the absolute height of the radiosonde.

The precision of temperature and geopotential height as a function
of pressure was evaluated from data reported at mandatory pressure
levels (850 mb, 700 mb, 500 mb, etc.) by calculating the rmsd at each
level. Past studies of the precision of constant pressure level data
have been performed by Rapp (1952), Lenhard (1970,1973) and Hoehne
(1980). Rapp evaluated data to 300 mb from a small number (six) of
dual radiosondes. He estimated standard errors in temperature which
ranged from 0.4-0.8°C; standard errors in geopotential height ranged
from 4-14 m. Lenhard analyzed the data taken from radiosondes
launched at the same time but separated by 16-19 km. He arrived at
an rms temperature difference of 0.2-0.3°C by fitting the observed
rms height difference with a calculated theoretical value. After
assuming a certain pressure error, he determined what temperature
error would be needed to arrive at that best fit. Hoehne used
differences between paired radiosondes to calculate a temperature
rmsd of 0.61°C and a geopotential height rmsd of 24 m.

Figure 3.1 shows the rms temperature differences calculated from
the dual radiosondes of this study as a function of pressure. They
are on the order of 0.35 K-0.4 K throughout the troposphere and increase
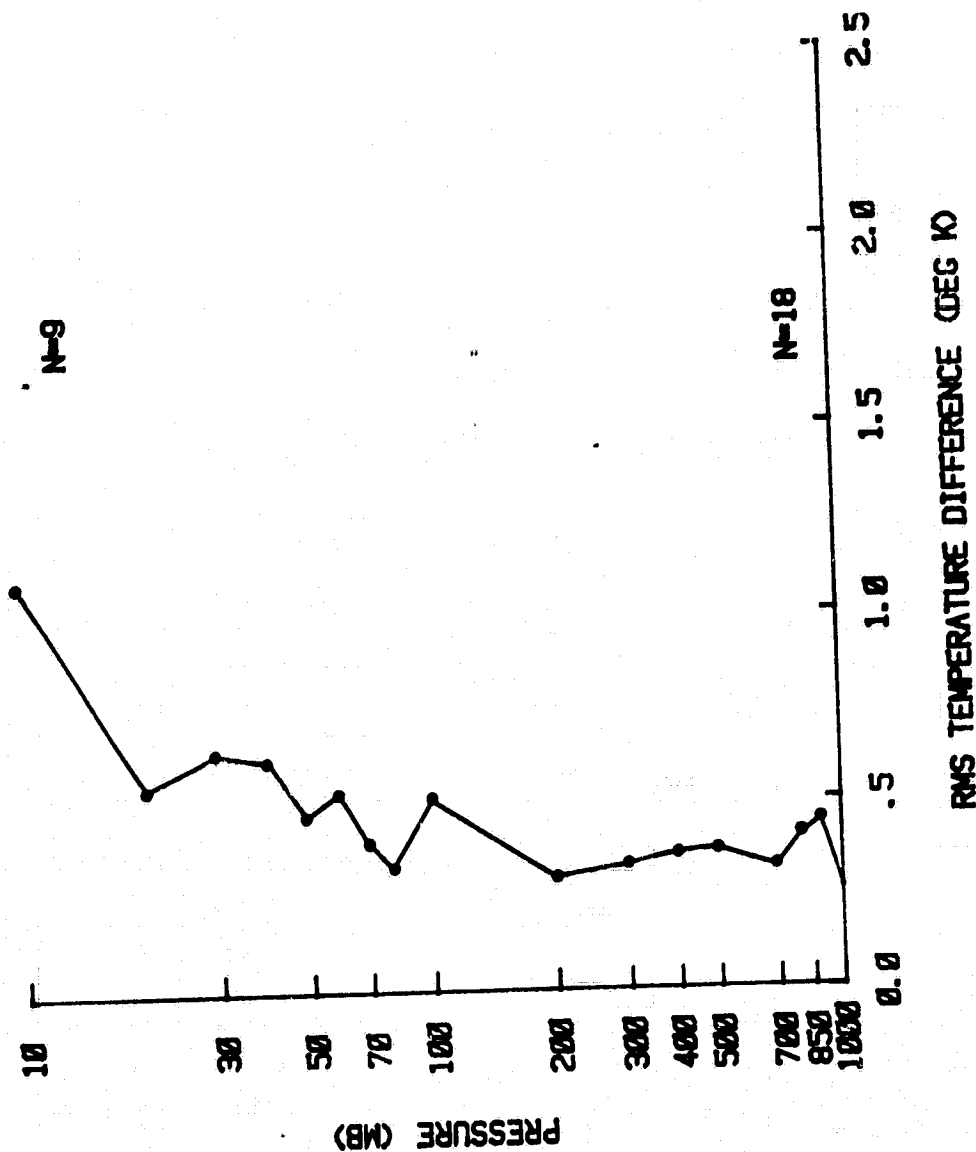
Figure 3.1 Rms temperature difference between N paired radiosondes
as a function of radiosonde-measured pressure.

to near 1.0 K as the upper stratosphere is reached. By summing squared temperature differences over all levels, an rms temperature difference of 0.46 K is obtained. The vertical profile of the rms geopotential height differences is shown in Figure 3.2. The rmsd continually increases with decreasing pressure and reaches 45 m at the 10 mb level. At each level, the rms difference is small relative to the height of the pressure level in question. Averaged over all levels, the rms difference is 20 m, in agreement with Hoehne. The rmsd computed at tropospheric pressures also agrees well with the results of Rapp. The radiosonde, therefore, shows good precision in the determination of the height of a constant pressure surface. It provides useful data for synoptic-type purposes.

Radiosonde precision can be investigated further by obtaining rms differences for temperature and pressure at common calculated heights. In the same study mentioned before, Hoehne (1980) calculated rms pressure and temperature differences according to height. He obtained values of 0.7 mb and 0.8°C, respectively, averaged over all levels. In this study, temperature and pressure values for each sounding were interpolated to every 500 m height increment. Rms temperature and pressure differences between paired radiosondes are presented in Figures 3.3 and 3.4, respectively. Temperature differences are on the order of 0.4 K up to 25 km, but increase quickly and reach over 1 K at 32 km. Averaged over all levels, the temperature rmsd is 0.5 K. The pressure rmsd taken over all levels is 0.3 mb with the largest value of 0.5 mb occurring at about 10 km. Figure 3.4 again shows the pressure-height determination to be highly precise; the radiosonde provides precise data for synoptic purposes.
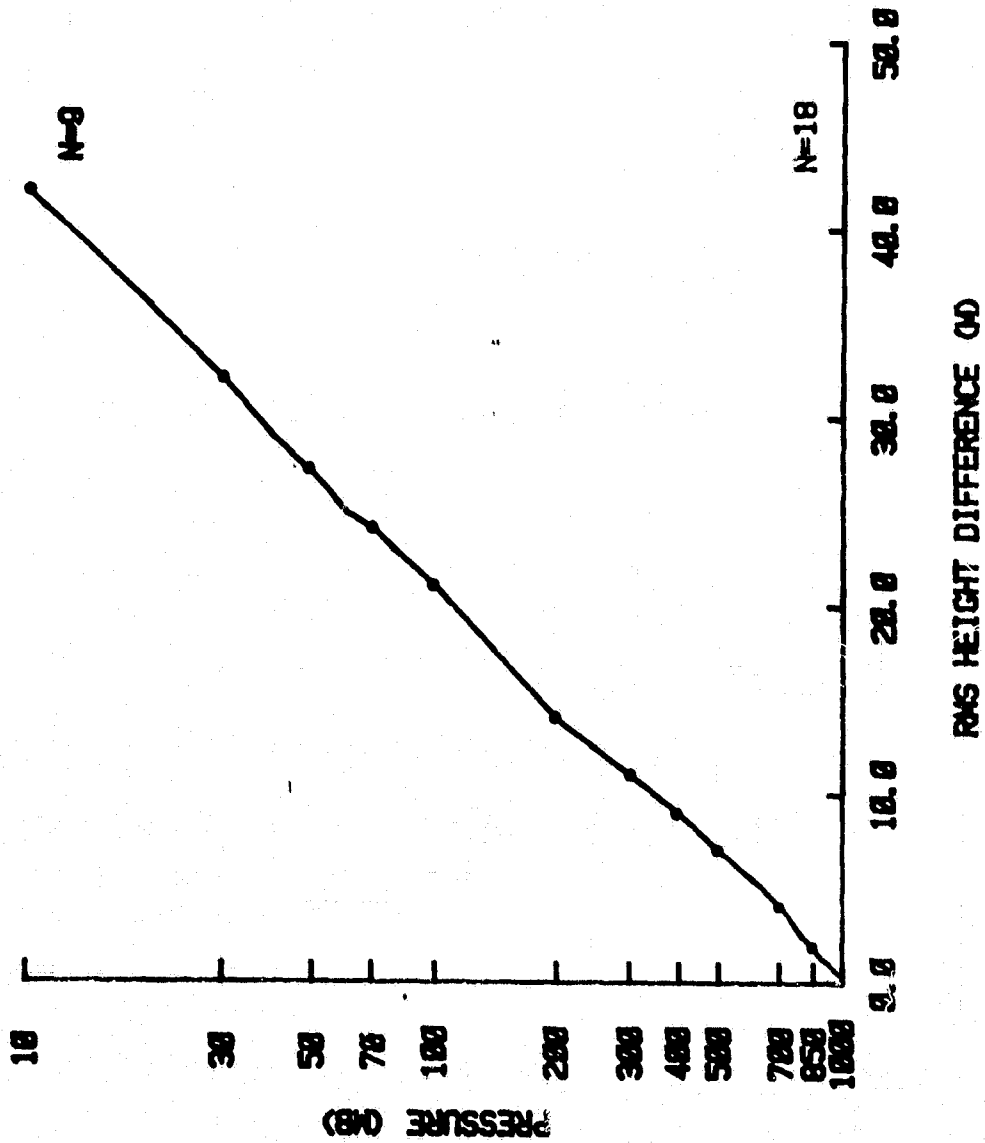
Figure 3.2 Rms height difference between N paired radiosondes as a function of radiosonde-measured pressure.
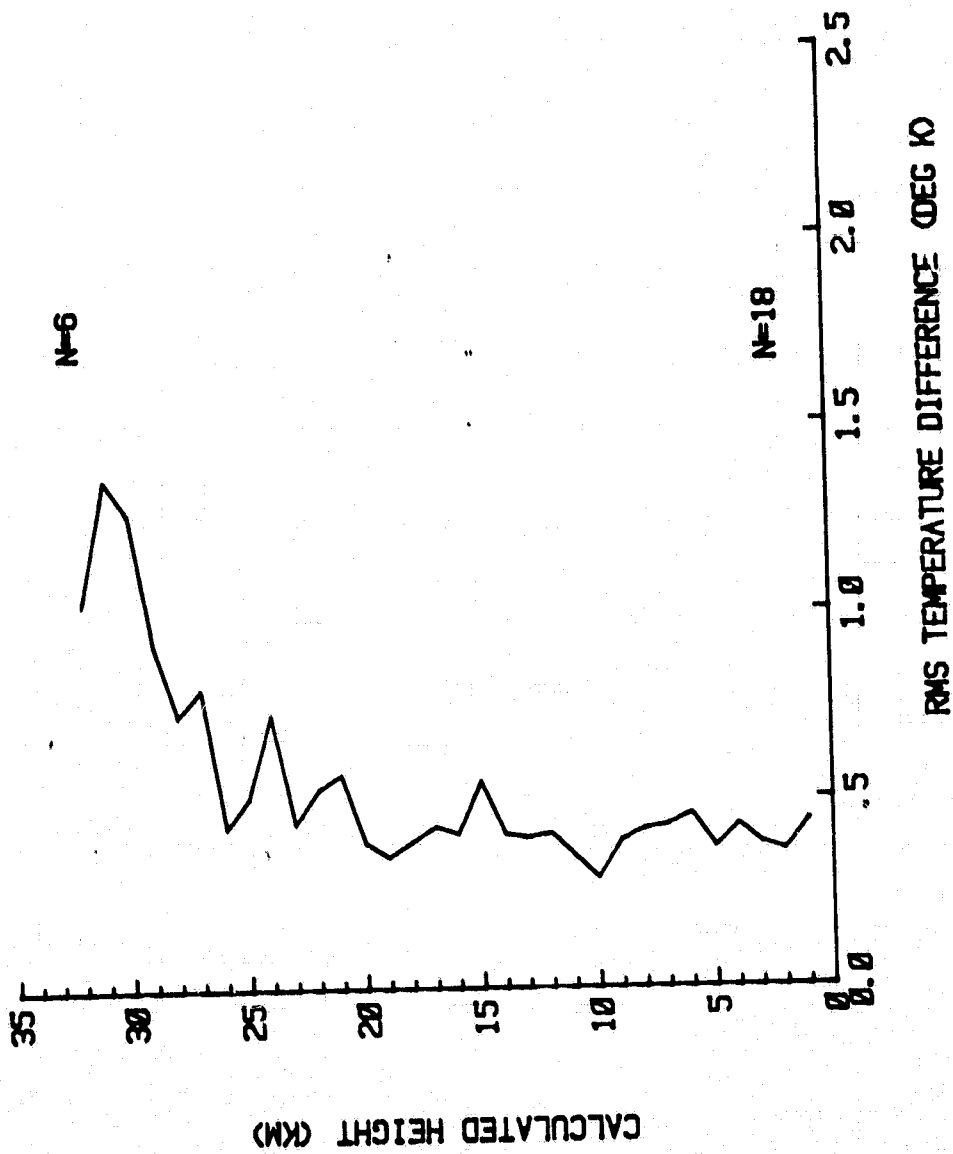
Figure 3.3 Rms temperature difference between N paired radiosondes
as a function of calculated radiosonde height.
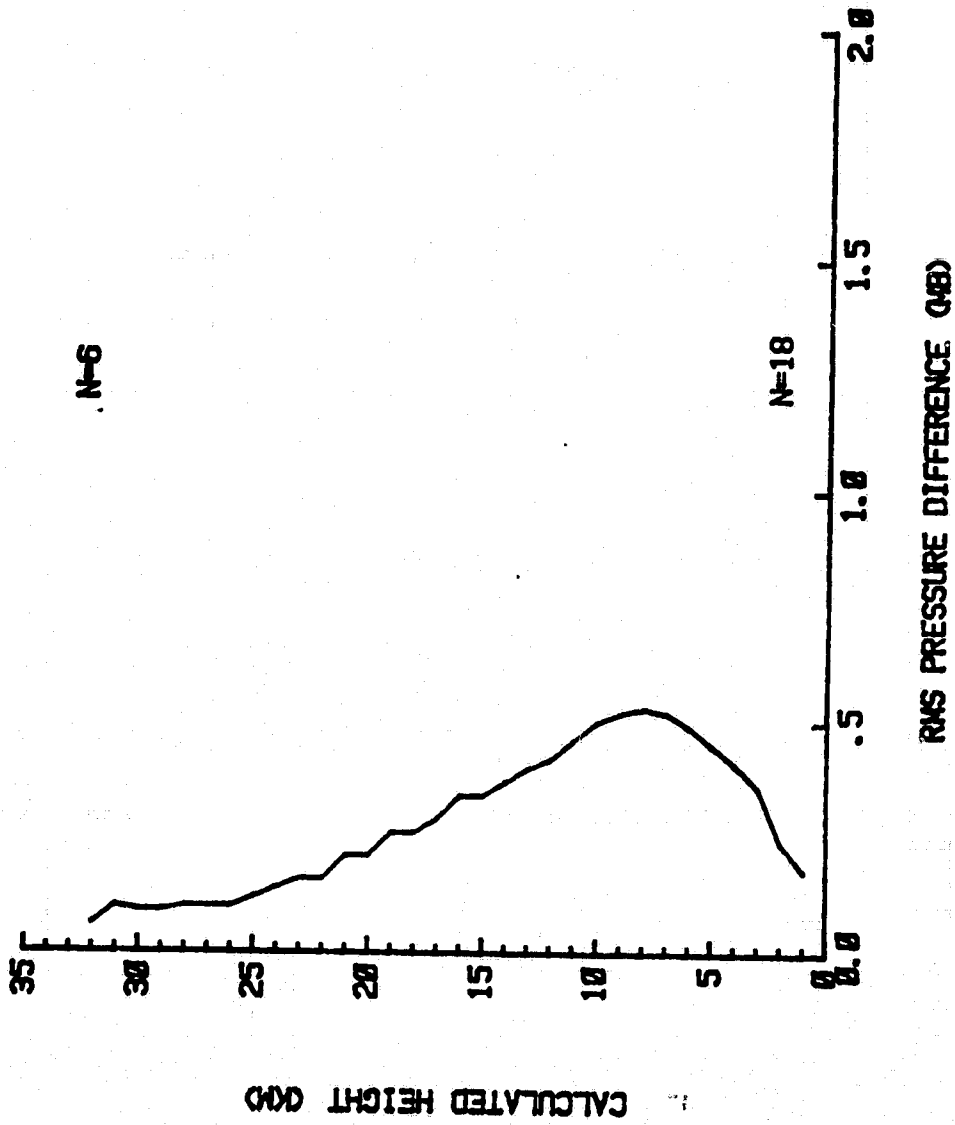
Figure 3.4 Rms pressure difference between N paired radiosondes
as a function of calculated radiosonde height.

It should be recognized that the above statistics are not necessarily indicative of the true radiosonde precision; regardless of the dual radiosonde configuration, the radiosondes may not be at the same location in the atmosphere when differences are taken at constant pressure or height. Because of errors in the pressure and temperature, the height calculated for each radiosonde is different from that of its partner; it also differs from the actual height of the radiosonde at that point in time.

The true precision can be evaluated by taking differences as a function of height as independently determined from the radar. This height is measured independent of temperature and pressure. The resultant temperature-height and pressure-height profiles are representative of the conditions at the dual radiosondes' actual location in the atmosphere. Since the same height is assigned to each radiosonde at the same time, any differences between the dual radiosondes are instantaneous differences calculated at the same point in the atmosphere; the actual precision can be determined.

Rms differences were calculated at every 500 m radar-height intervals. Figure 3.5 shows the precision of temperature as a function of radar height to vary little with altitude. Squared differences summed over all levels give a rmsd of 0.46 K. This small rmsd is similar to the results of Hodge and Harmantas (1965), who calculated instantaneous differences from paired radiosondes and obtained a temperature precision of 0.51°C. Hoehne (1980) used the same technique to arrive at a precision of 0.67°C. The improved precision found in this study could result from the very careful data reduction employed. Notice also in Figure 3.5 that there is no large increase
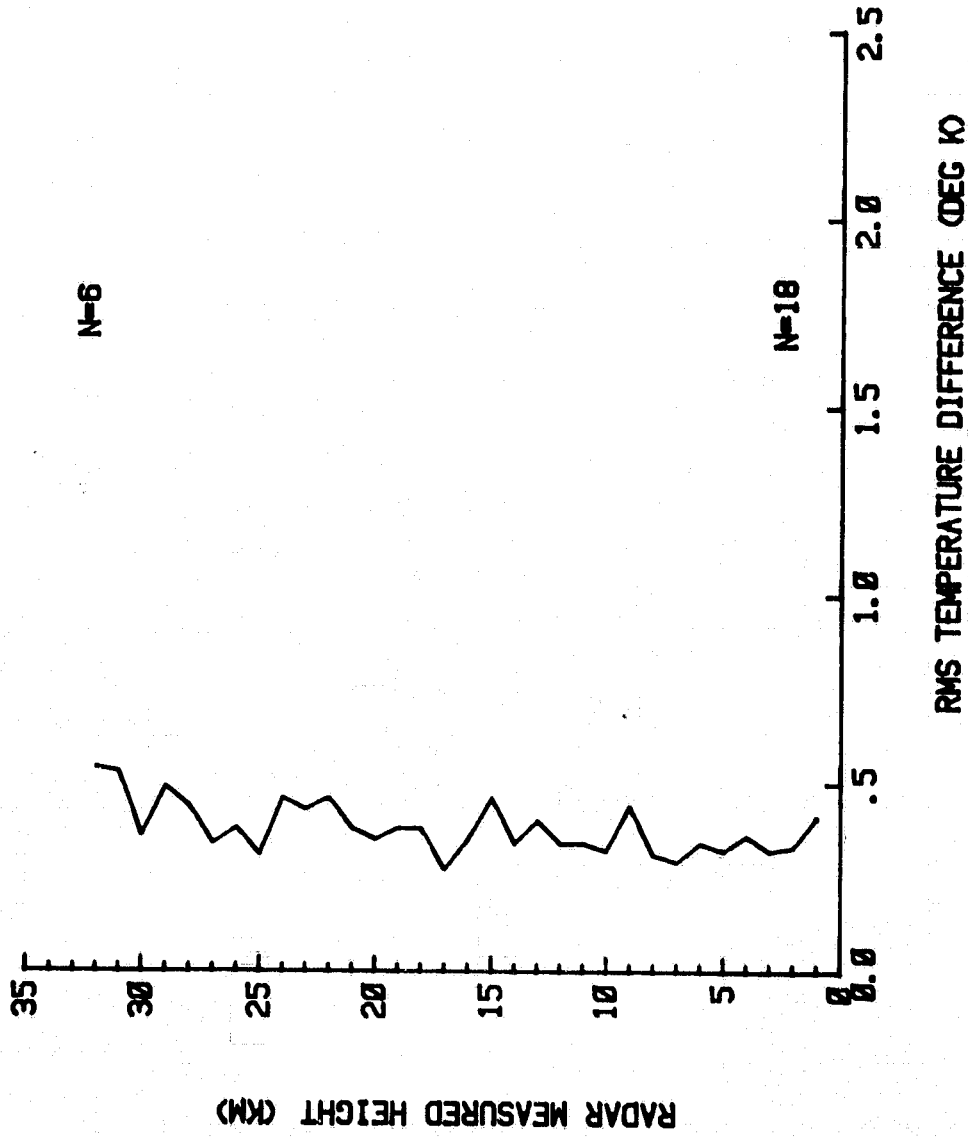
Figure 3.5 Rms temperature difference between N paired radiosondes as a function of radiosonde height as determined by radar.

in the rmsd as the end of the flight approaches, a pattern contrary
to the previous precision calculations (Figures 3.1 and 3.3). It
can be concluded that much of those increases were probably due to
the radiosondes sensing different levels of the atmosphere rather
than the same level.

The rms pressure differences as a function of radar height are
shown in Figure 3.6. The rmsd reaches 2.0 mb near 30 km and never
falls below 1.0 mb at any level. Evaluated over all levels, the
pressure rmsd is 1.45 mb. This result is quite different than the
rmsd as a function of calculated height (Figure 3.4). As with the
temperature precision, the pressure precision decreases if one
examines instantaneous differences for which both radiosondes are
at the same point in the atmosphere at the same time. The results
of Hoehne (1980) agree with this conclusion. Hoehne's findings
and those of this study are presented in Table 3.1, which shows that
the precision of radiosonde data differs depending upon the means by
which the data is evaluated.

While the true precision of the temperature measurement is rather
good, the large rms pressure differences can introduce large errors
in the instantaneous or actual height of the radiosonde. This point
can be investigated through comparisons between calculated radiosonde
heights and radar-measured radiosonde heights. Figure 3.7 shows the
rmsd[1] between the two methods of height determination plotted versus
radar-measured height (assumed to be the actual height of the radio-

---

[1] Since identical instruments are no longer being compared, the rmsd
is no longer a measure of precision; rather, it is now a measure of
the spread of the differences between measurements.
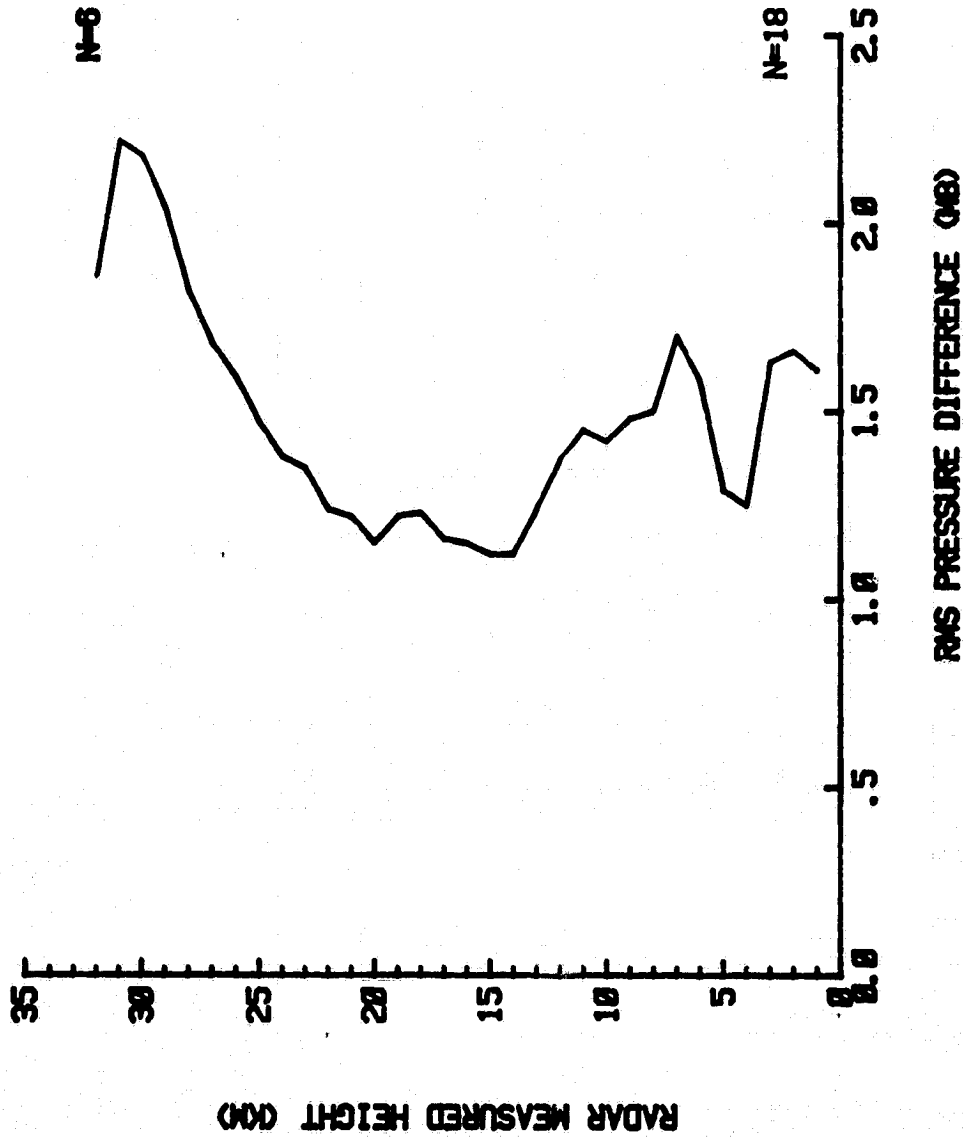
Figure 3.6 Rms pressure differences between N paired radiosondes as a function of radiosonde height as determined by radar.

Table 3.1 Precision of radiosonde data.*

Statistics calculated as function of	Rms temp. difference (K)		Rms pressure difference (mb)	
	This Study	Hoehne (1980)	This Study	Hoehne (1980)
Pressure	0.46	0.62	–	–
Geopotential Height	0.5	0.84	0.34	0.72
Radar-determined Geopotential Height (time)	0.46	0.67	1.45	1.9

*Rmsd calculated by summing squared differences over all levels.
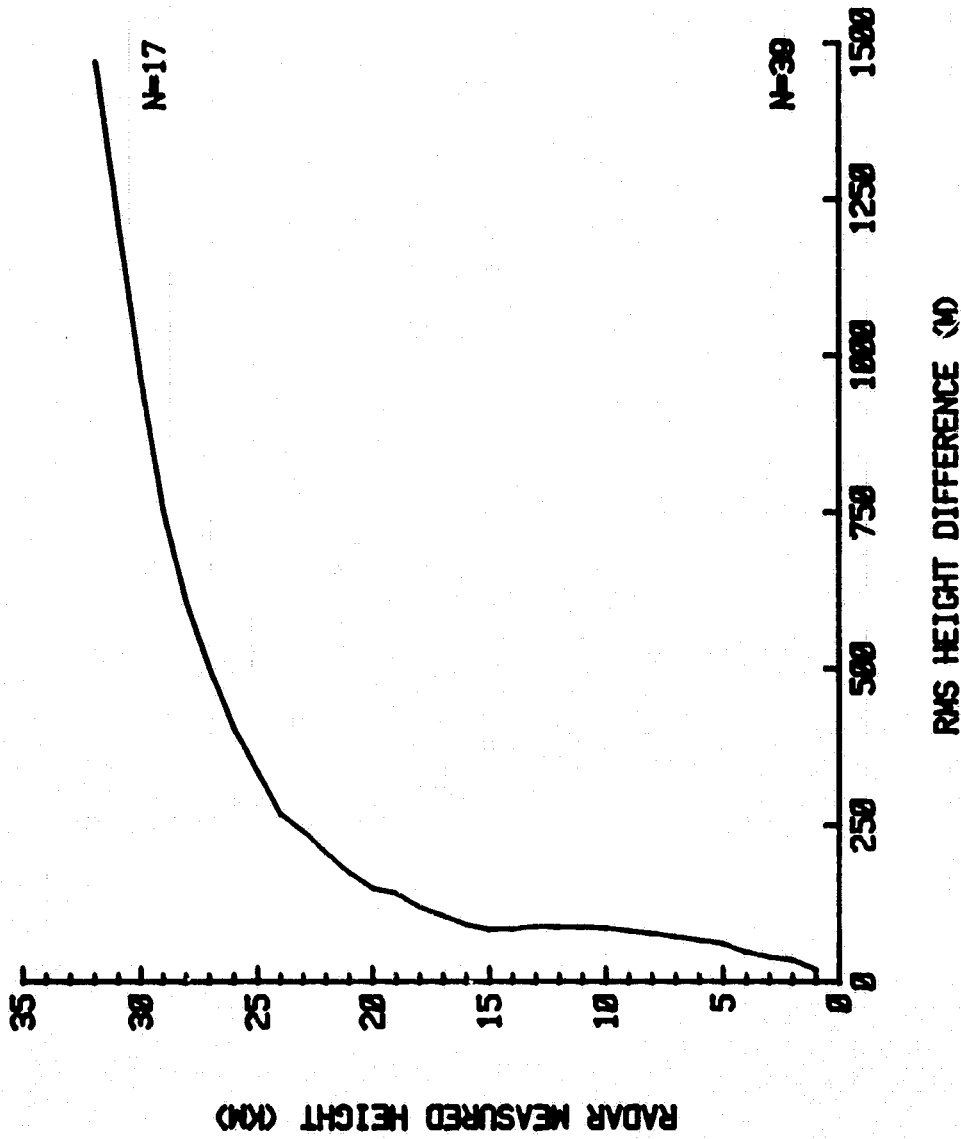
Figure 3.7 Rms differences between radiosonde height measured by radar and calculated with the hypsometric equation. N is the total number of radiosondes used for the comparison.

sonde at any time). Extremely large rms differences are prevalent with values of near 1500 m at 32 km. Closer inspection of the data revealed that two radiosondes had suffered aneroid cell malfunctions which caused large pressure differences ($\sim$ 4 mb) late in their flights. This resulted in calculated heights which differed from the radar heights by up to 3000 m and contributed greatly to the large rmsd. While the discrepancies in pressure and height would probably be noticed on a synoptic analysis and ultimately smoothed out, they would not be apparent to a user examining a single, stand-alone profile such as in a comparison of a radiosonde sounding to a satellite sounding. Extraordinary measures (dual radiosondes and radar) were needed to identify and isolate a radiosonde with a malfunctioning aneroid. For these reasons, the malfunctioning radiosondes were not removed from the sample. Figure 3.7 shows that there is a large discrepancy between the actual location of the radiosonde in the atmosphere and where it is calculated to be. The imprecision of the radiosonde measurements, particularly of pressure, is to blame. It must be emphasized again that this does not detract from the radiosonde's usefulness in assigning a precise height to a constant pressure surface.

The pressure measurement may be investigated further by using the radar heights and radiosonde temperatures to calculate the pressure at any time in a manner similar to that used for the rocketsonde. The excellent approximation

$$P_{calc_N} = P_o \exp\left[-\sum_{i=1}^{N} \frac{g_o \, \Delta z}{R\overline{T}_{vi}}\right] \tag{3.3}$$

is used where P_{calc} is the calculated pressure at the top of a layer

Δz (taken from radar), P_o is the pressure at the layer bottom, g_o is

9.8 ms^{-2}, R is the dry gas constant, and $\overline{T}_v$ is the mean virtual

temperature in the layer. Since we are using precise temperatures

and a single radar measurement, these calculated pressures are very

precise. Table 3.2 shows that the precision of the calculated pressure

is no worse than 0.45 mb. The differences were taken as a function

of time so they are indeed instantaneous. Comparison of the actual

measured pressures with the calculated pressures is shown in Figure 3.8.

Average differences reach 1.0 mb with the rmsd about 1.5-2.0 mb. Keep

in mind that the comparison of this calculated pressure with the

measured pressure says nothing of the accuracy of P_{calc} because, as

we have seen, the measured pressure is by no means the actual pressure.

The advantage of P_{calc} is that it is more precise than the measured

pressure when time or instantaneous height is the independent variable.

Table 3.2 Precision of P_{calc}

P_{calc} (mb)	Rmsd (mb)
10	.08
30	.14
50	.19
70	.23
100	.28
200	.37
300	.42
400	.44
500	.43
700	.34
850	.20
1000	.02
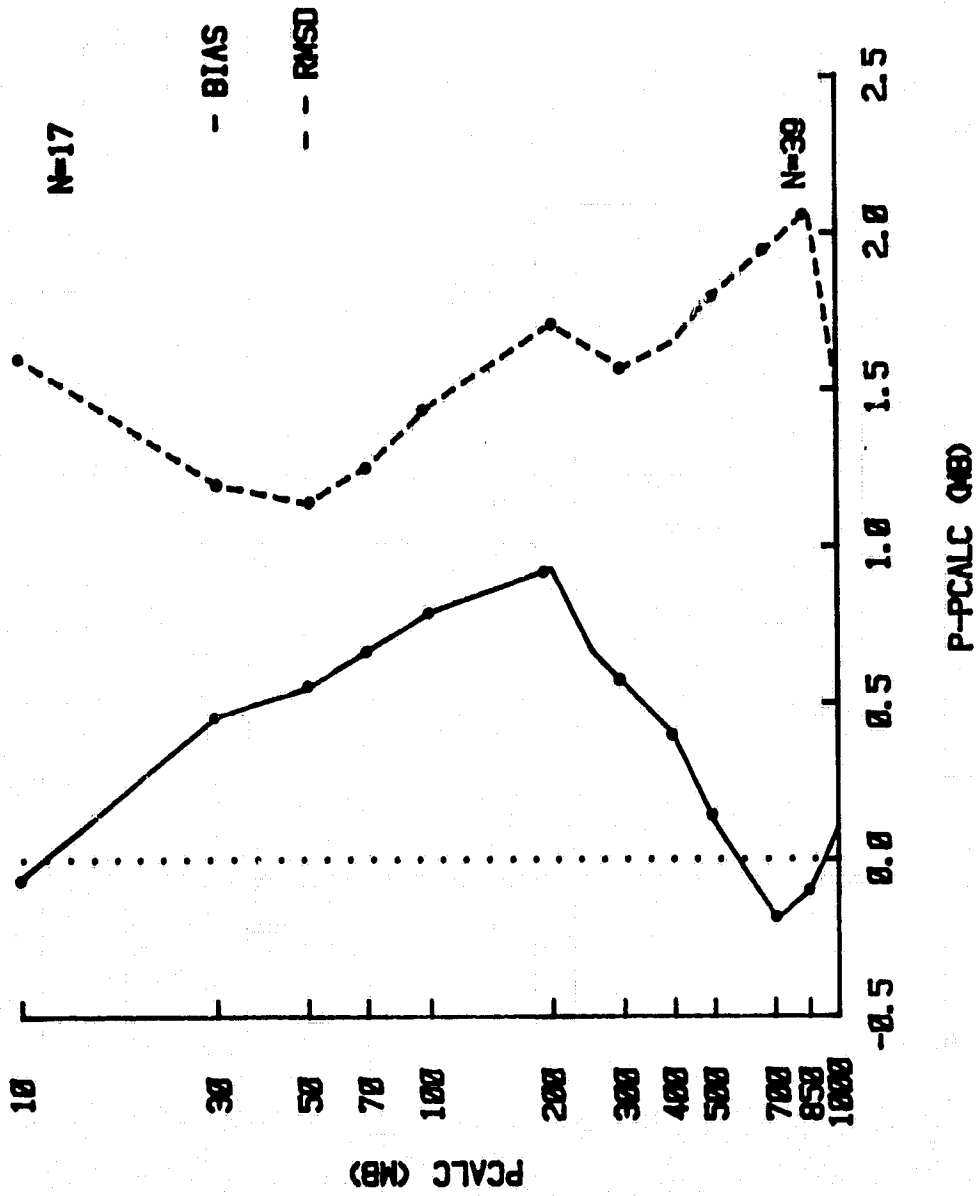
Figure 3.8 Average difference (bias) and rmsd between radiosonde-
measured pressure and calculated pressure. N is the
total number of radiosondes used in the comparison.

As a final comparison, pressure-height profiles were generated using the radar heights and calculated pressures. These profiles were compared with the pressure-height profiles taken directly from the radiosonde data. The statistics are given in Figure 3.9. It is seen that the two types of profiles are remarkably similar; small biases and small rms differences occur throughout the entire profile. These results again show that while the radiosonde cannot be located at the correct (instantaneous) pressure-height point, it can estimate the correct profile, a characteristic which again illustrates the usefulness of the radiosonde for synoptic-type purposes. For single station, non-synoptic purposes where the radiosonde data is considered absolute, variability in the pressure measurement results in large displacements from the actual altitude of the radiosonde. This problem can be overcome, however, through the use of radar-tracking to provide precise pressures and true heights.

Because the dual radiosonde wind data were not processed, the precision of radiosonde wind measurements will not be examined here. Since satellite-derived winds will be compared to radiosonde winds, however, it is still necessary to have an idea of the repeatability of the radiosonde winds. Bauer (1976) investigated the variation between radiosonde wind data at one point in the atmosphere and wind data in the surrounding atmosphere. A wind report at a particular station was chosen to be the "base" wind. Components of winds reported within 660 km of the base wind report were then extrapolated to the base wind location. Differences between the extrapolated wind components and the base wind components were calculated; standard deviations of approximately 6 ms^{-1} and 8 ms^{-1} were found for the u and v components, respectively.
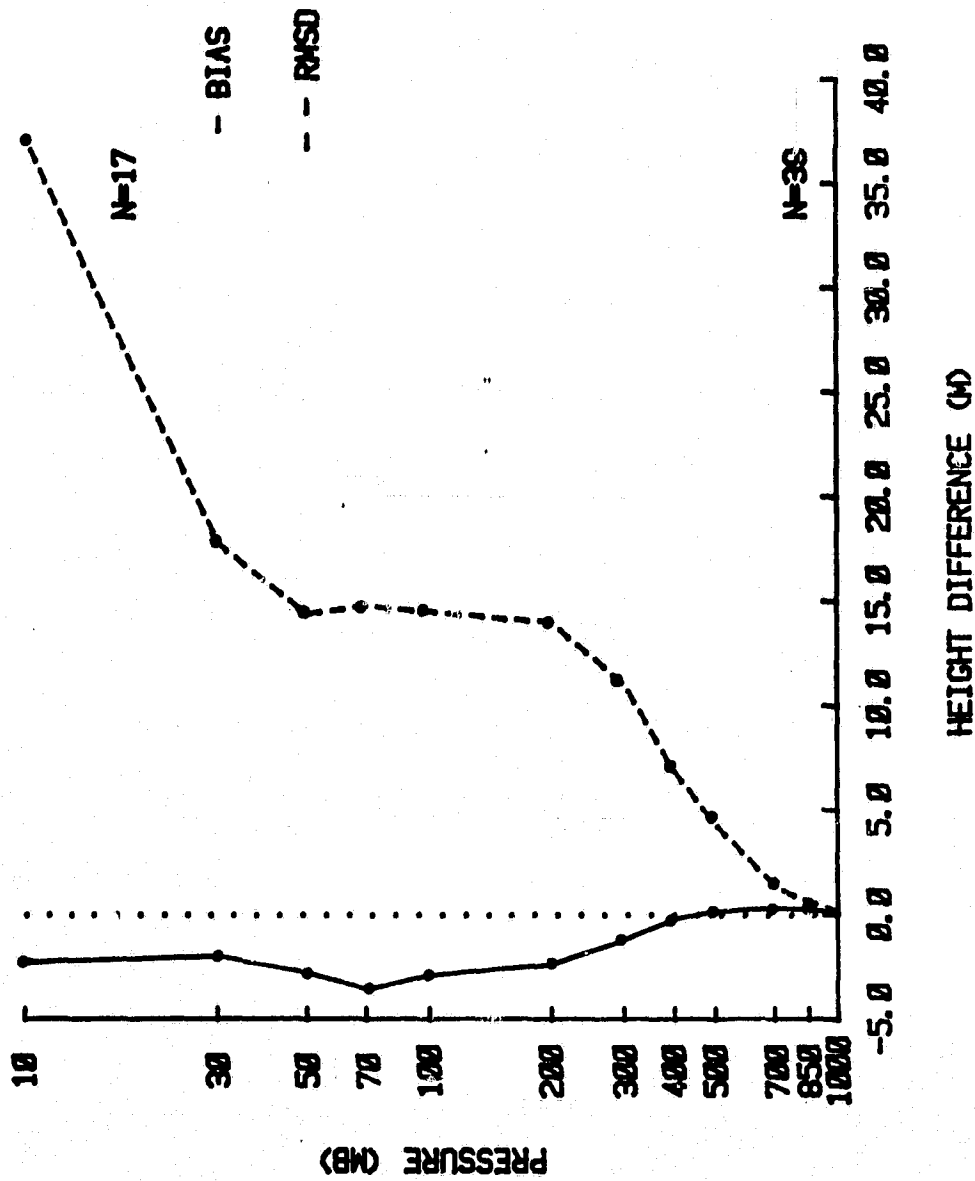
Figure 3.9   Average difference (bias) and rms height difference
between radiosonde-calculated height at measured
pressure and radar-measured height at calculated
pressure. N is the total number of radiosondes
used in the comparison.

3.3 Rocketsonde Precision

Investigators of rocketsonde precision usually examine the precision of the temperature measurement as a function of height. Miller and Schmidlin (1971) used temperature measurements made five minutes apart up to 55 km to calculate an average temperature rmsd of 1.08°C. In a recent study, Schmidlin evaluated the rmsd for forty-five pairs of rocketsondes with time differences of five minutes to one hour. From the lowest altitude reported up to 53-55 km, the rmsd changed little, but increased exponentially above 55 km. Schmidlin speculated that this increase could have been caused by atmospheric variability at very small time scales, instrumental problems, or the sensitivity of the temperature corrections to flight-related parameters such as anomalous fall velocities. After forming regression relations (time structure functions) between mean squared temperature differences and the time separation between rocketsonde launches, Schmidlin extrapolated the relation to zero time difference (simulating simultaneous measurements) and arrived at an rms difference of 0.8°C at 35 km which increased to 1.3°C at 50 km. Values of precision were not calculated above 55 km.

Similar estimates of the rocketsonde temperature precision were obtained from this study by calculating rms differences between rocketsondes launched five minutes apart. The lack of a large sample size prohibited us from adopting Schmidlin's technique. It has already been noted earlier in this chapter that due to experimental design, differences between paired rocketsondes consist of not only instrumental variability, but also of atmospheric spatial and temporal variability. However, if the statistics calculated from the present

study are to be used as estimates of precision, it must be assumed that the atmosphere did not vary during the paired rocket flights. Table 3.3 shows the agreement between rms temperature differences calculated by Schmidlin (1981) and the rms temperature differences calculated in this study. Figure 3.10 presents the rms temperature differences plotted versus height at 1 km intervals. Small changes in the rmsd are present below about 55 km. The rmsd rapidly increases height above 55 km. This is consistent with the findings of Schmidlin (1981). Squared temperature differences summed over all levels below 55 km result in a temperature rmsd of 1.8 K; above 55 km they result in a temperature rmsd of 5.7 K. While the large variability above 55 km is cause for concern and should be investigated further, it creates no problems in this study since rocketsonde temperatures up to only around 55-56 km will be used for comparison with satellite temperatures.

Table 3.3   Rocketsonde rms temperature differences
calculated by Schmidlin (1981) and calculated
in this study from measurements made five
minutes apart.

Height (km)	Schmidlin (1981) °C	This Study °C
55	1.3	1.6
50	1.3	1.1
45	1.2	1.2
40	1.0	1.0
35	0.8	0.9
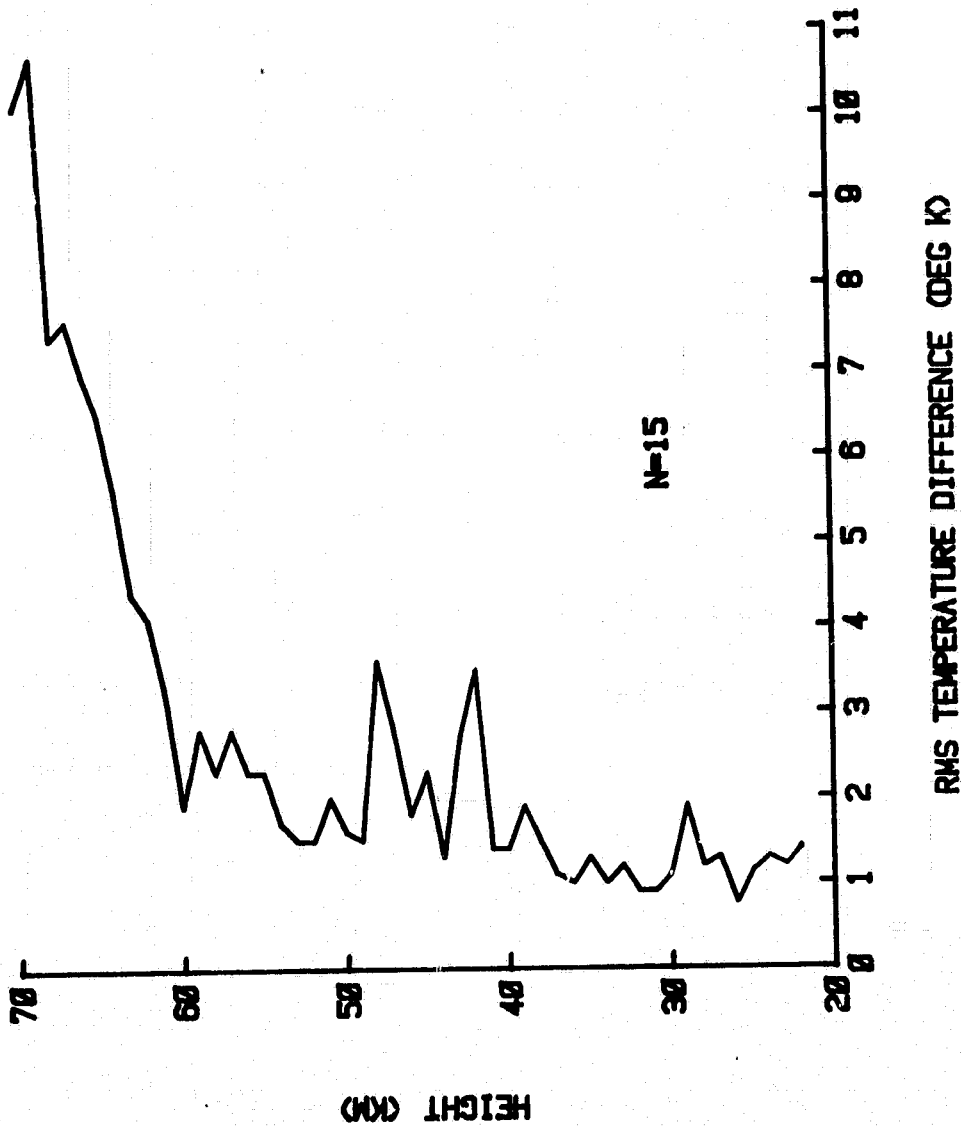
Figure 3.10 Rms temperature difference for N paired rocketsondes
as a function of geometric height.

An additional comparison dealt with the precision of the rocket-sonde geopotential heights of the 10 mb, 5 mb, 2 mb, 1 mb, and 0.4 mb pressure surfaces. The geometric rocket altitudes were converted to geopotential heights with Equation 3.2 and were used with the calculated rocketsonde pressures to logorithmically interpolate the heights to the desired pressure. Values of the rms differences between geopotential heights of paired rocketsondes are given in Table 3.4.

The multiple rocketsonde flights also enabled us to estimate the precision of the wind data. A cubic spline was fitted to the reported wind data and evaluated at the previously mentioned pressures. The rms differences for the u and v components are listed in Table 3.5. These values tend to reflect the precision of the tracking radar used (in this case, the FPS-16). The use of less precise radars (e.g. SPANDAR) would result in a larger rmsd. Additionally, differences tend to be larger at the topmost levels of the rocketsonde flight (Miller and Schmidlin, 1971).

Table 3.4   Rms geopotential height differences between
rocketsondes launched five minutes apart.

Pressure (mb)	Rmsd (m)	N (pairs of rocketsondes)
0.4	199	15
1	195	15
2	187	15
5	173	15
10	177	13

Table 3.5   Rms differences between wind components of
rocketsondes launched five minutes apart.

Pressure (mb)	Rmsd (ms^{-1})		N (pairs of rocketsondes)
	u	v	
0.4	1.9	2.4	15
1	1.2	1.2	15
2	1.5	1.3	15
5	1.2	1.0	15
10	1.1	0.7	13

4.0 SATELLITE - IN SITU MEASUREMENT COMPARISONS

4.1 Experiment Design

Overpasses of the NOAA-6 satellite on ten dates (within the period of February 1980 to May 1980) provided soundings of mean layer temperature (TOVS points) in a 10° latitude by 10° longitude area around Wallops Island. These layers are bounded in the vertical by pressure surfaces of 1000, 850, 700, 500, 400, 300, 200, 100, 70, 50, 30, 10, 5, 2, 1, and 0.4 mb. Figure 4.1 illustrates a typical distribution of the TOVS points around Wallops Island. As noted earlier, atmospheric temporal and spatial variability are a concern in satellite - in situ intercomparisons since soundings from the two instruments are usually made neither at the same place nor at the same time. The dual radiosondes previously described were launched approximately two and one-half hours before the satellite overpass. The rocketsondes were launched, on average, fifteen minutes before overpass. A typical duration of the in situ flights in terms of their time proximity to the NOAA-6 overpass is shown in Figure 4.2. We assumed that the large scale atmospheric structure did not vary between the times of the in situ launches and the NOAA-6 overpass. While it would have been preferable to have had smaller radiosonde-satellite time differences, the lack of a sufficient number of GMD's at Wallops Island necessitated that a radiosonde flight be ended before a rocketsonde could be flown. The only way to accomplish this was to launch the radiosondes two and one-half hours before the satellite overpass.

To minimize spatial variability, a Cressman interpolation scheme (Cressman, 1959) was applied to the TOVS point data. Four scans
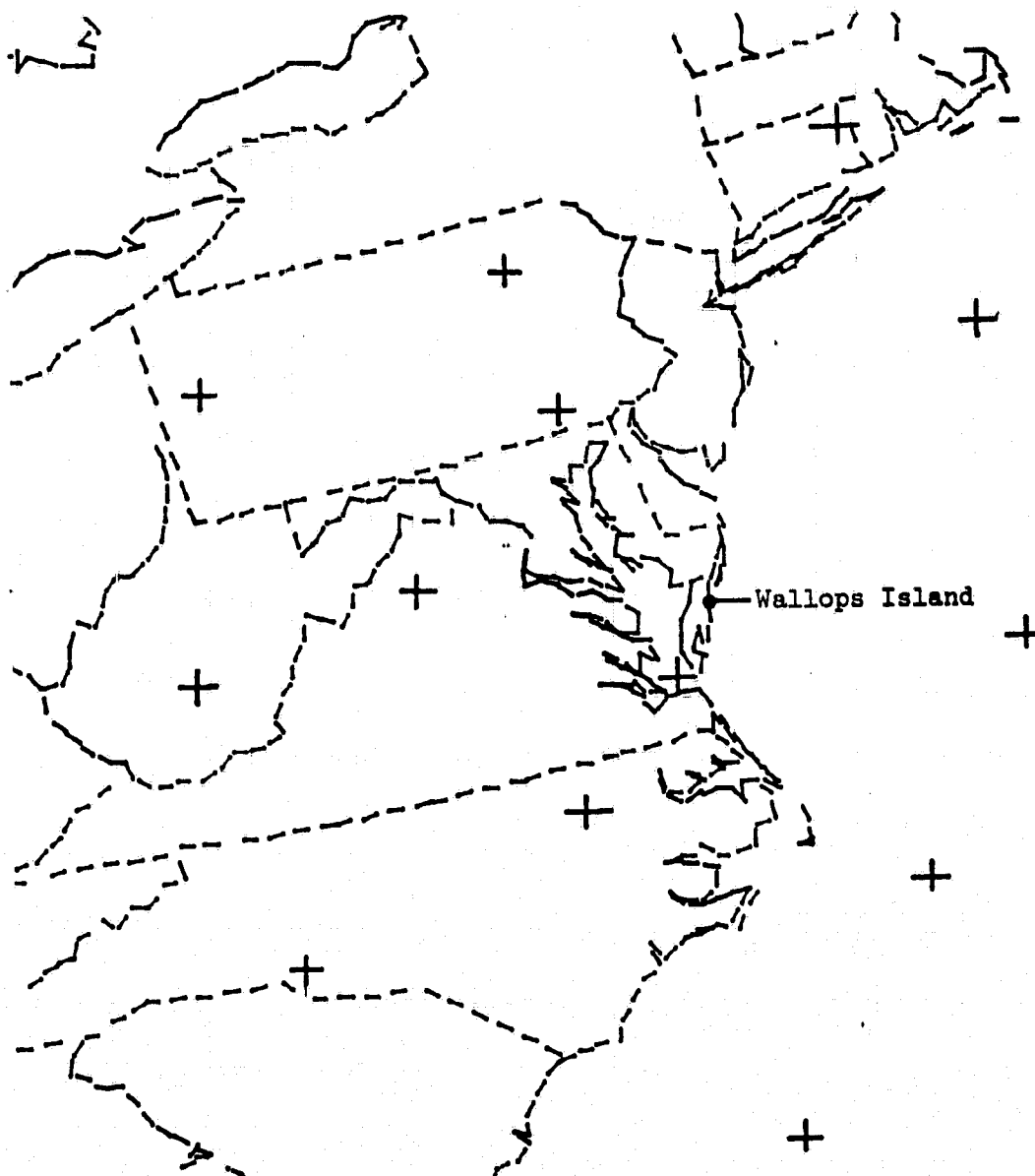
Figure 4.1 Typical distribution of TOVS points around Wallops Island,
Virginia.
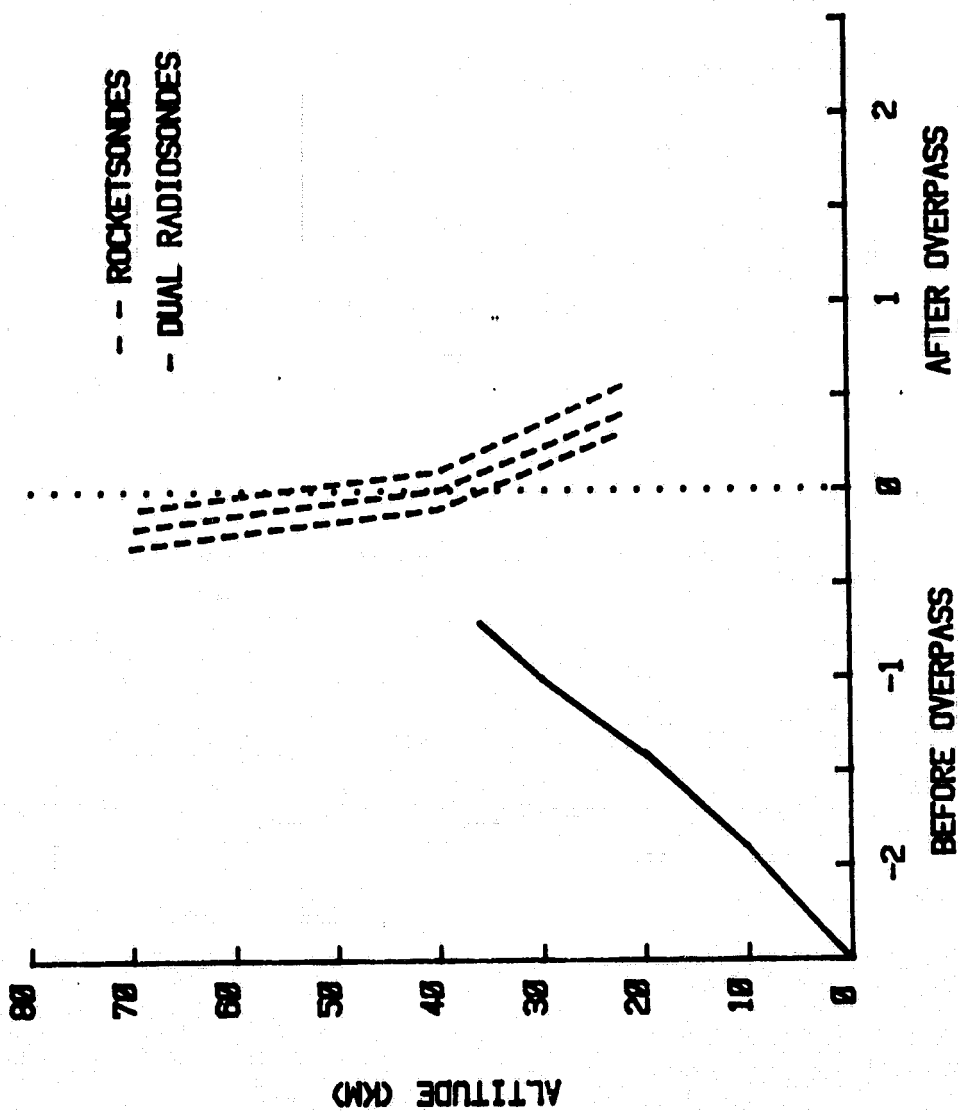
Figure 4.2 Typical duration of the in situ flights in terms of their time proximity to the NOAA-6 overpass.

with a radius of maximum influence of 4° latitude were used to interpolate the TOVS points in the surrounding area to the Wallops Island location. This provided a weighted-average temperature sounding up to 0.4 mb to be compared to in situ soundings.

Another difficulty with satellite - in situ comparisons is that the measurements themselves have characteristically different spatial sensitivities. In Chapter 2, it was noted that the satellite produces a volume-averaged measurement while in situ instruments produce point measurements. Differences will arise not only because of errors in the satellite and/or in situ sensors, but also because two essentially different measurements are being compared. Bruce et al. (1977) have investigated the disagreement between satellite and radiosonde temperature profiles that results from radiosonde error and the difference in the area of each measurement. They calculated differences of up to 1.4 K between a hypothetical area-averaged satellite sounding and a radiosonde sounding located at the center of the radiometrically viewed area.

4.1.1 Statistical Technique

It can be assumed that the observed differences between satellite and in situ instruments come from errors in the satellite measurements themselves, errors in the in situ measurements, and effects from atmospheric variability. Thus,

$$\sigma_T^2 = \sigma_{SAT}^2 + \sigma_I^2 + \sigma_{ATM}^2 \qquad (4.1)$$

where σ_T^2 is the total calculated variability (the mean square difference or rmsd^2) between satellite and in situ measurements, σ_{SAT}^2 is the

variability due to satellite errors, σ_I^2 is the variability due to a
single <u>in situ</u> instrument error, and σ_{ATM}^2 is atmospheric variability.
Since temporal variability between soundings was ignored and spatial
variability between soundings was minimized with the Cressman scheme,
σ_{ATM}^2 is assumed to be zero. Equation 4.1 may be solved for σ_{SAT}, i.e.

$$\sigma_{SAT} = (\sigma_T^2 - \sigma_I^2)^{1/2} \tag{4.2}$$

where σ_{SAT} will be considered to be the root-mean-square error (rmse)
due to the satellite alone. The quantity σ_I^2 will be obtained by
using the results of Chapter 3. Those results gave the rmsd between
paired instruments; the variability attributed to a single instrument
can be calculated by assuming that the total mean square difference
is composed of independent and equal errors in each of the instruments.
Then,

$$\sigma_{TI}^2 = 2\sigma_I^2 \tag{4.3}$$

where σ_{TI}^2 is the total mean square difference between paired <u>in situ</u>
instruments. Furthermore,

$$\sigma_I^2 = \sigma_{TI}^2/2 \tag{4.4}$$

and

$$\sigma_I = \sigma_{TI}/\sqrt{2} \tag{4.5}$$

where σ_I is the root-mean-square error of single in situ measurement.
Equation 4.4 will be used with (4.2) to assign rms errors to the
satellite measurements.

4.2 Satellite-Radiosonde Comparisons

4.2.1 Mean Layer Temperature

There are few published studies which have dealt with the
comparability of temperature soundings from the newer satellites
(TIROS-N and NOAA-6) to "ground truth" data. Those that have been
published, however, provide background on the relative error character-
istics of the satellite and on the effect of retrieval methods on
those error characteristics.

Smith et al. (1979) presented a statistical comparison between
interactive computer-processed TIROS-N soundings and operational radio-
sonde soundings over North America for a one-month period. Figure 4.3
shows rms temperature differences between radiosonde soundings and
satellite soundings derived from clear and partially cloudy retrievals
(labeled HIRS in Figure 4.3); rms differences between radiosondes
and satellite soundings taken from cloudy retrievals are labeled as
MSU. Largest rms differences occur at the surface and at the tropo-
pause region for reasons which will be discussed later. Note also
that the cloudy retrievals produce soundings which are less accurate
(higher rmsd) than soundings from clear and partially cloudy retrievals.
This is because the fewest channels (all microwave channels and HIRS-2
channels 1, 2, 3, and 17) are used for cloudy retrievals than for any
other retrieval.
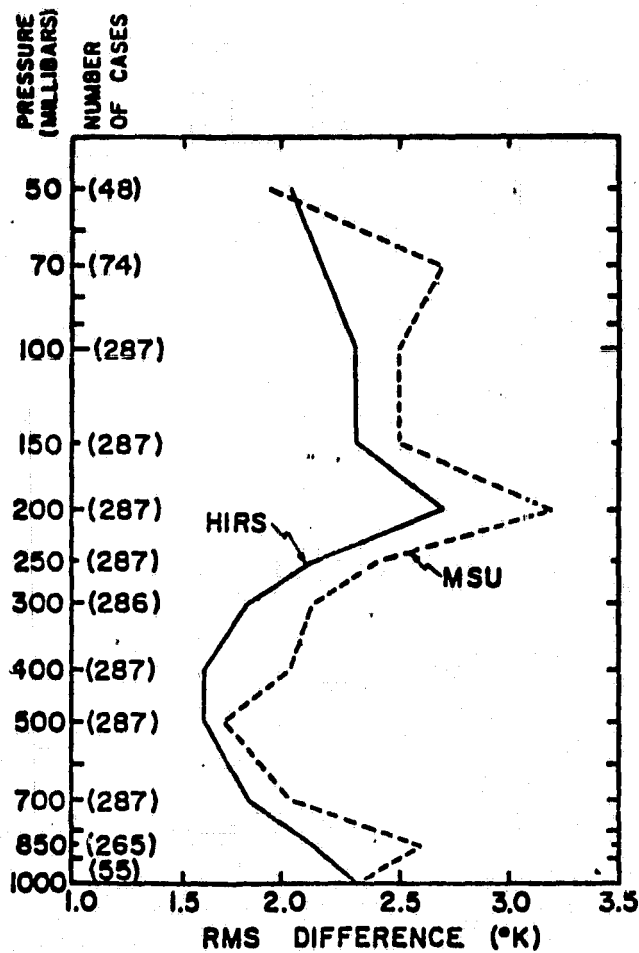
Figure 4.3 Rms temperature difference
between interactively derived
TIROS-N soundings and radio-
sonde soundings from 22 March -
19 April 1979 (from Smith et al.,
1979).

Phillips et al. (1979) also examined the effect of retrieval
techniques by calculating mean and rms differences between clear,
partly cloudy, and cloudy soundings and radiosondes. Table 4.1
summarizes their results of comparisons for a nine-month period
over North America. The largest rms differences again occur for
the cloudy retrieval. Rms differences calculated for clear retrievals
tend to be smallest in the lower troposphere. One would expect that
corrections for clouds would reduce the accuracy of the satellite
sounding, so clear retrievals should have the lowest rms differences
of the three retrieval methods throughout the troposphere. However,
rms differences for the partly cloudy (N*) retrievals tend to be less
than those of the clear retrievals in the mid to upper troposphere.
Phillips et al. (1979) attributed this contradiction to possible
cloud contamination of some of the clear soundings and also to the
mixing together of clear and N* retrievals to generate the regression
coefficients used to convert radiances to temperatures.

Finally, Schlatter (1981) compared TIROS-N mean layer virtual
temperatures to National Meteorological Center (NMC) objective
analyses over much of the continental United States and parts of
southern Canada. His results are given in Figure 4.4. Average
differences show the satellite temperatures to be higher than the
analyzed temperatures near the surface and near the tropopause, and
lower through the middle troposphere. Largest rms differences are
near the surface. Schlatter also found no large rms differences at
tropopause levels. Rms temperature differences stratified by retrieval
method agree with the results from Phillips et al. (1979). Cloudy
soundings generally have largest rms differences, while partly cloudy

Table 4.1   Results of satellite-radiosonde intercomparisons
            of mean layer temperature over North America
            (from Phillips, et al., 1979).

Layer (mb)	Mean Difference (°K) (Sat-Radiosonde)			rmsd (°K)		
	Clear	N*	Cloudy	Clear	N*	Cloudy
1000-850	-0.7	1.0	1.1	2.8	3.3	2.4
850-700	0.1	0.9	-0.6	1.8	2.4	2.5
700-500	-0.4	0.5	-1.7	1.9	1.1	2.5
500-400	-0.5	0.5	-1.5	1.9	1.5	2.6
400-300	-0.2	-0.4	-0.8	1.9	1.5	2.6
300-250	0.0	-0.8	0.0	2.1	1.9	2.6
250-200	0.7	0.0	1.3	2.3	1.6	2.4
200-150	0.5	1.8	2.0	2.5	3.4	3.2
150-100	-0.3	0.5	0.5	1.6	1.6	1.6
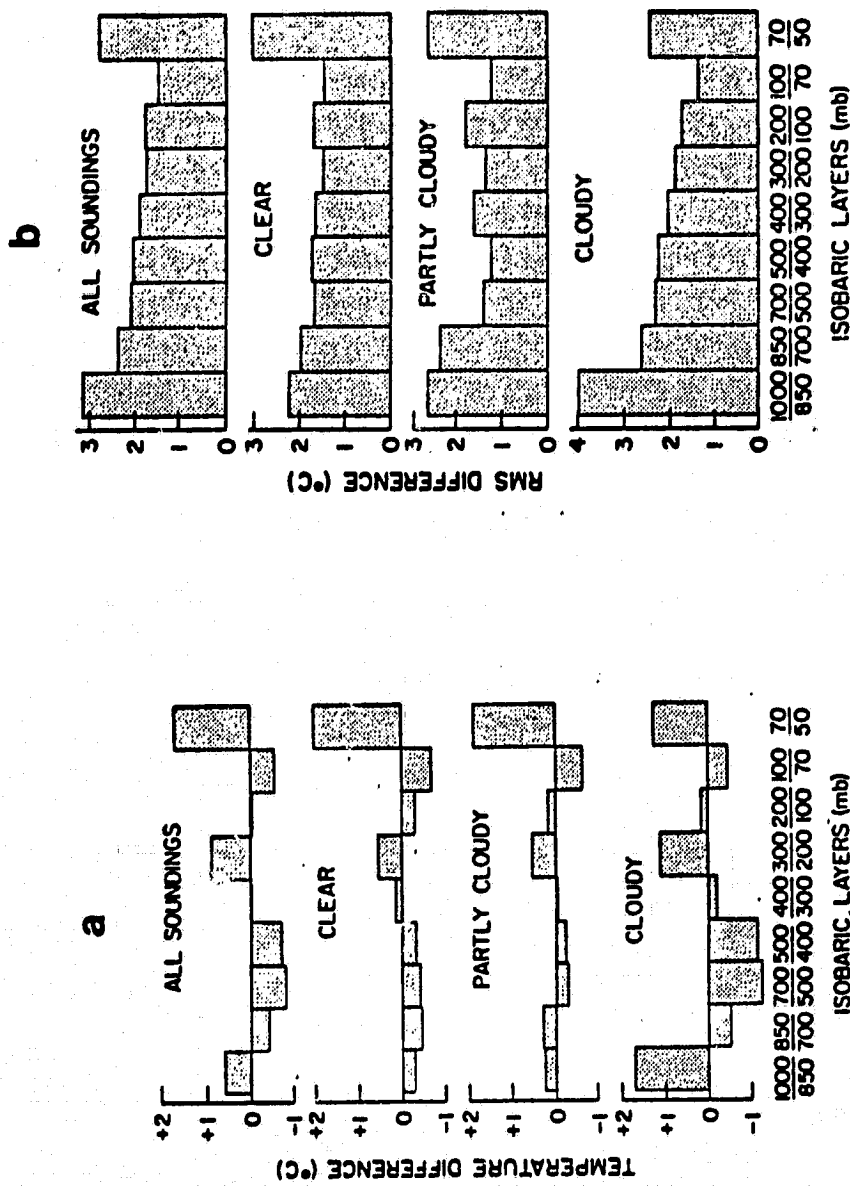
Figure 4.4 Average difference (a) and root-mean-square difference (b) between TIROS-N and objectively analyzed mean layer virtual temperatures, stratified by retrieval method (from Schlatter, 1981).

soundings tend to have smaller rms differences than clear soundings in the mid to upper troposphere.

While the above studies note that errors are present in the in situ measurements, they do not consider quantitatively the influence of these errors on the rms differences. The special flights from Wallops Island enabled us to isolate in situ measurement errors and to examine their impact on satellite - in situ measurement comparisons. As mentioned earlier, it is felt that the verifying radiosonde data used in this study are subject to less error than typical operational soundings. Thus, the "ground truth" data base used here is probably of higher quality than that of the above studies. Finally, the above studies examined a large number of soundings (e.g. Schlatter used 1514 soundings) which permitted the stratification of soundings by retrieval method while still maintaining a rather large sample for each method. The present study did not have the luxury of such large samples, so the intercomparisons were performed with no consideration given to the retrieval technique employed. The weighted satellite soundings at Wallops Island were produced by the Cressman interpolation of clear soundings, N* soundings, and cloudy soundings mixed together as they were reported.

Figure 4.5a and Figure 4.5b show typical comparisons of temperature profiles between NOAA-6 and the radiosondes of this study. The satellite mean layer temperatures are plotted at the centers of each layer, while the radiosonde temperatures are discrete temperatures reported at a given pressure. Although this could be considered a comparison of two different quantities, it nevertheless illustrates differences that would occur if a satellite sounding were directly

(b)
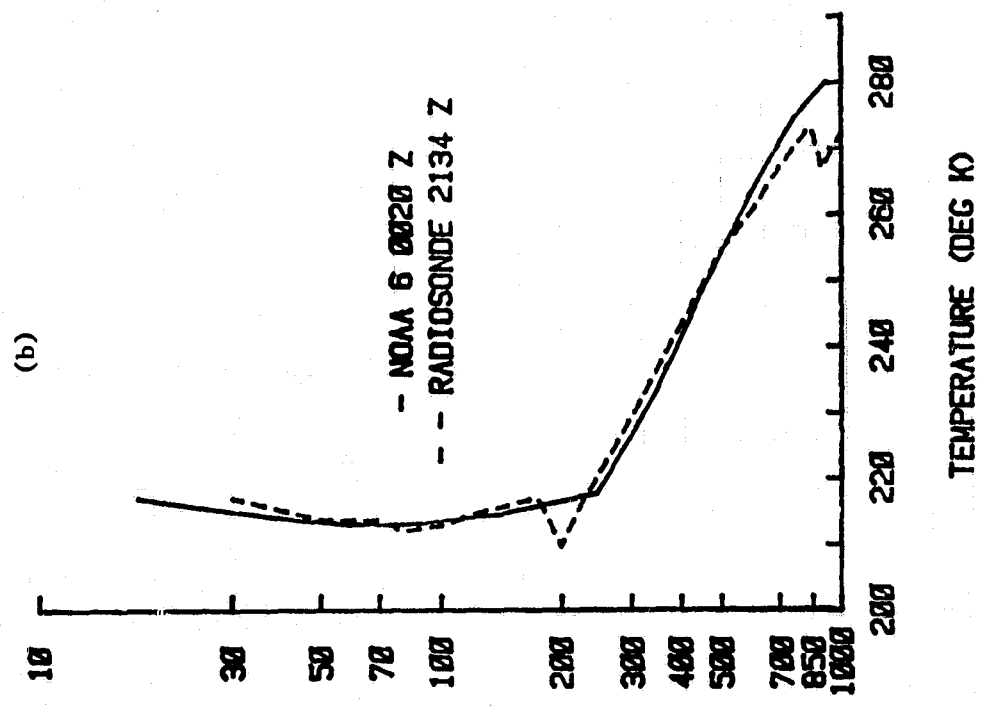
Figure 4.5b Weighted-average satellite temperature profile for 16 May 1980 and radiosonde temperature profile for 15 May 1980.

(a)
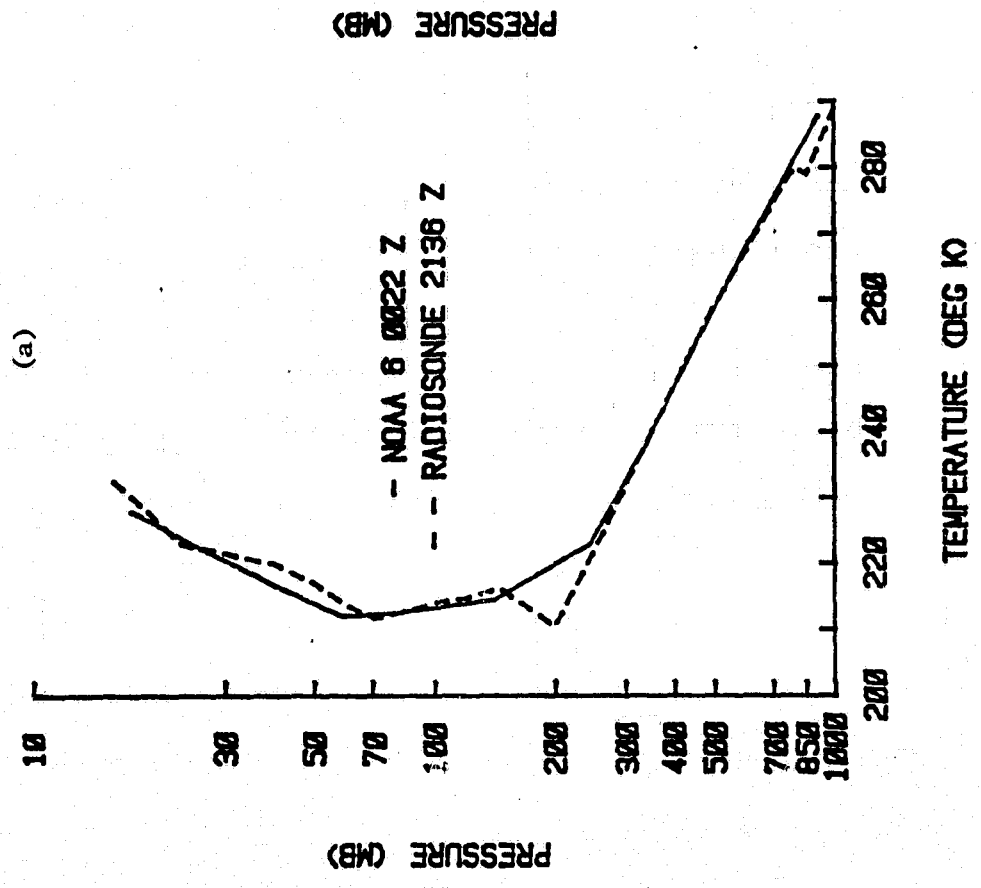
Figure 4.5a Weighted-average satellite temperature profile for 13 March 1980 and radiosonde temperature profile for 12 March 1980.

substituted for a radiosonde sounding. In both figures, note that while the general shape of the radiosonde profile is captured by the satellite, the detailed structure is not captured. This is evident in the tropopause region where the complex structure is smoothed out. In addition, the satellite tends to "see" a warmer tropopause region than does the radiosonde. Both figures also show that the satellite tends to smooth out common features near the surface such as temperature inversions. The above characteristics of the satellite soundings are caused in part by the broad weighting functions of the radiometers. Any small-scale structure in the temperature profile is not captured by the satellite. Temperature extremes like that at the tropopause are underestimated. In regions of little structure such as the mid-troposphere, the satellite reproduces the temperature structure rather well. Notice the agreement between profiles at 400-600 mb in Figures 4.5a and 4.5b.

Statistical comparisons between satellite mean layer temperatures $\overline{T}_{SAT}$ and mean layer temperatures calculated for each radiosonde are presented in Figure 4.6. Temperature differences ΔT are defined as

$$\Delta T = \overline{T}_{SAT} - \overline{T}_I \qquad (4.6)$$

Here $\overline{T}_I$ is the radiosonde mean layer temperature. The rms error attributed to the satellite is calculated using Equation 4.2. As noted, the largest rms errors occur in the lowest layer (1000-850 mb) and in the tropopause region. Values of 1.8 K to 2.2 K rmse are seen in the mid troposphere, while the smallest rmse of about 1.3 K - 1.5 K occurs above 100 mb. These patterns are consistent with the
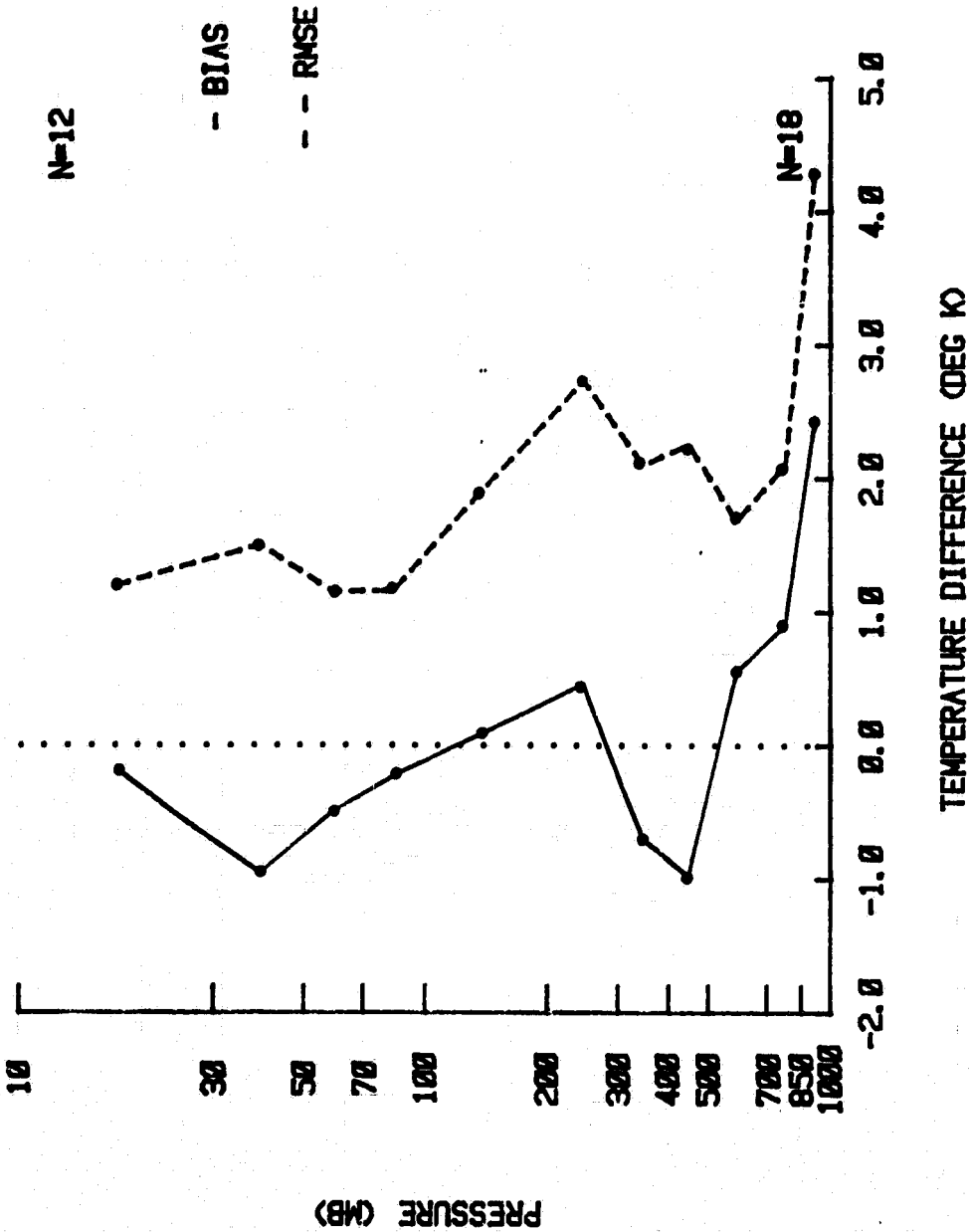
Figure 4.6 Average differences or bias (satellite-radiosonde) for
N comparisons between satellite and radiosonde mean
layer temperature, and the root-mean-square error
attributed to the satellite.

results of Broderick et al. (1981) and of Smith et al. (1981). The mean difference curve in Figure 4.6 shows that the satellite-retrieved temperatures are higher than the temperatures from the dual radiosondes in the low troposphere and near the tropopause; lower temperatures are found in the middle troposphere. The warm bias at low levels has also been seen by Schlatter (1981) (Figure 4.4), but the warm bias found in this study extends to higher levels. Finally, the satellite mean layer temperature tends to be lower than that of the radiosonde above 100 mb.

The effect of imprecision in the radiosonde data has little influence on the rms error assigned to the satellite. Table 4.2 gives the rmsd between satellite and radiosonde mean layer temperatures, the rmse in layer mean temperature for a single radiosonde, and the satellite rms error. The rmse for a single radiosonde is small compared to the total rms difference.

The effect of using the Cressman interpolation to minimize spatial variability between the locations of the TOVS points and the radiosondes can be examined by comparing rms differences calculated using interpolated satellite mean layer temperatures to rms differences calculated using the TOVS point closest to Wallops Island. These points were, on average, 125 km from Wallops Island. Table 4.3 shows that a minor reduction in the mean layer temperature rmse of the satellite is achieved when a weighted-average (or interpolated) satellite sounding, rather than an actual sounding located relatively close to the verifying radiosonde, is compared to that radiosonde sounding.

Table 4.2 Comparison between the root-mean-square difference
(rmsd) between satellite and radiosonde mean layer
temperatures to the root-mean-square error (rmse)
in mean layer temperature for a single radiosonde
and for the satellite.

Layer (mb)	rmsd (K)	Radiosonde rmse (K)	Satellite rmse (K)
30-10	1.20	0.37	1.14
50-30	1.50	0.32	1.46
70-50	1.15	0.27	1.12
100-70	1.16	0.23	1.13
200-100	1.94	0.24	1.92
300-200	2.77	0.20	2.72
400-300	2.10	0.24	2.10
500-400	2.25	0.28	2.25
700-500	1.68	0.22	1.67
850-700	2.10	0.28	2.09
1000-850	4.24	0.34	4.23

Table 4.3 Comparison of satellite mean layer temperature
root-mean-square error calculated by using a
weighted-average satellite sounding and by
using the TOVS point closest to Wallops Island.

Layer (mb)	rmse (K) (Weighted Average Sounding)	rmse (K) (Closest TOVS Point)
30-10	1.20	1.00
50-30	1.50	1.57
70-50	1.15	1.11
100-70	1.15	1.44
200-100	1.94	2.18
300-200	2.77	2.88
400-300	2.10	2.13
500-400	2.25	2.71
700-500	1.68	2.70
850-700	2.10	3.31
1000-850	4.24	5.21

4.2.2 Geopotential Height

Geopotential heights of various pressure surfaces were calculated at each TOVS point by using the reported mean layer temperatures in the hypsometric equation. It should be noted that moisture data were not reported for most of the TOVS points used in this study, thus kinetic temperature rather than virtual temperature was used to calculate the satellite geopotential heights. Since the mean layer temperatures are taken over such deep layers, it is believed that only minor differences in the satellite geopotential heights resulted from the exclusion of moisture (Moyer et al., 1978). Sample calculations show the errors due to the omission of moisture to be about 2 m at 850 mb and to accumulate to 15 m at 300 mb.

The lowest layer in which data from NOAA-6 are reported is 1000-850 mb. To derive the heights of any pressure surface above 1000 mb, the height of the 1000 mb surface must first be determined. Sea level pressure and temperature were taken from hourly surface airways observations and interpolated to the TOVS point locations. Assuming a standard lapse rate of $6.5°C$ km^{-1}, the hydrostatic equation was integrated from sea level pressure to 1000 mb (Carle and Scoggins, 1981) to yield

$$z_{1000} = \frac{T_o}{\Gamma} \left[1 - \left(\frac{1000}{P_o}\right)^{R\Gamma/g_o} \right] \qquad (4.7)$$

where the variables are defined as follows:

z_{1000}: height of the 1000 mb surface

T_o: sea level temperature

Γ: standard lapse rate ($6.5°C$ km^{-1})

P_o: sea level pressure

R : dry gas constant (287 J Kg^{-1} K^{-1})

g_o: 9.8 ms^{-2}

The thicknesses derived from NOAA-6 mean layer temperatures were added to z to give the height of a pressure surface at each TOVS point. Those heights were then interpolated to Wallops Island with the Cressman scheme.

Figure 4.7 gives the bias (satellite-radiosonde) and the satellite rmse for geopotential heights at pressures from 850 mb to 10 mb. At tropopause levels, the satellite-derived geopotential heights range from 20 m to 30 m higher than those of the dual radiosondes. The mean layer temperature bias changes sign several times in the vertical; this has a compensatory effect on the bias in the height calculations, a feature also noted by Schlatter (1981). The generally negative temperature bias at stratospheric levels compensates for the generally positive bias at lower levels and results in height biases of less than 15 m at pressures above 30 mb. Note that the rmse continually increases with height until it attains 100 m at the 10 mb level.

The satellite-derived heights become less reliable with altitude. The relative difference, however, between the rmse and the height at which it is calculated at stratospheric levels is particularly small. Although the rmse is also relatively small at tropospheric levels, these differences could be important, particularly at the lowest levels.

Imprecision in the radiosonde geopotential heights has little influence on the comparisons. Table 4.4 provides a comparison of the
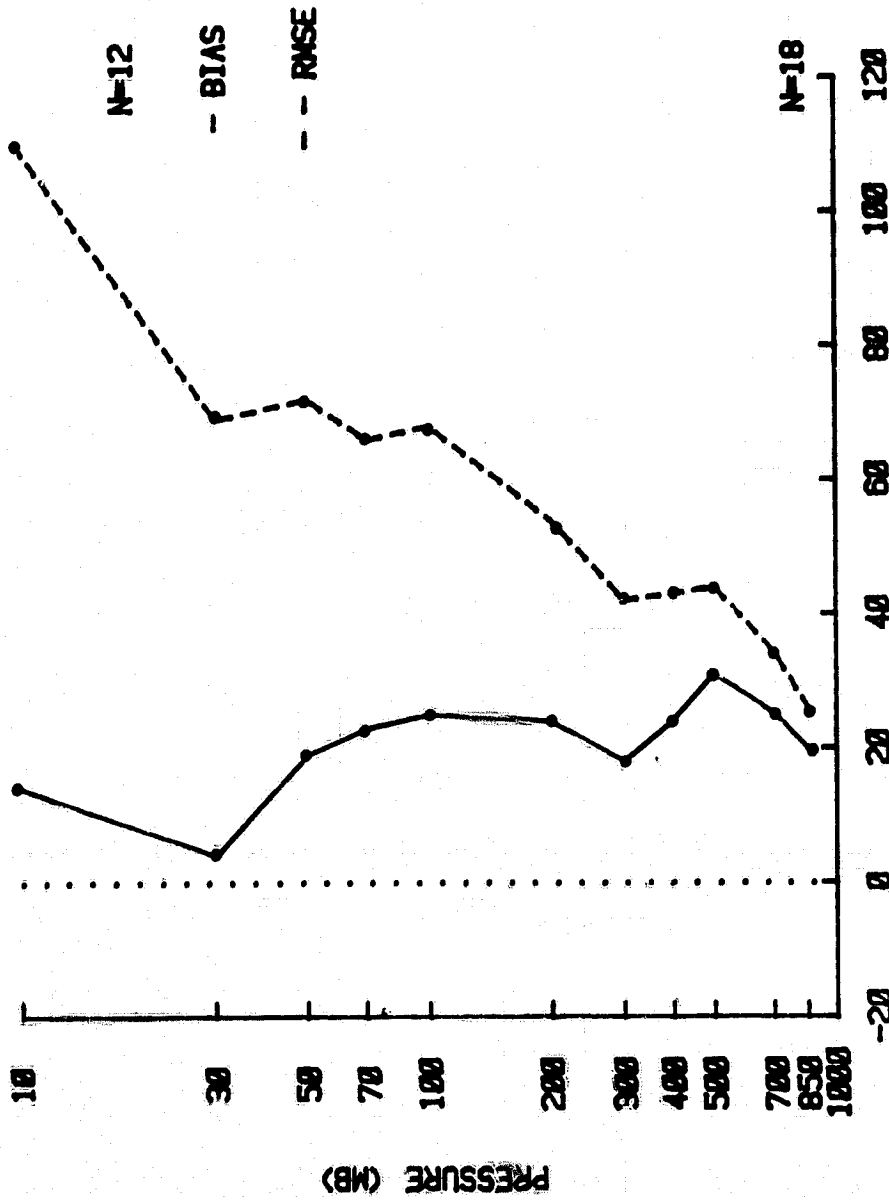
Figure 4.7 Average differences or bias (satellite-radiosonde) for
N comparisons between satellite and radiosonde geopotential
heights, and the root-mean-square error attributed to the
satellite.

Table 4.4 Comparison of root-mean-square differences (rmsd) between satellite-derived and radiosonde geopotential heights to the root-mean-square error (rmse) in geopotential height for a single radiosonde and for the satellite.

P (mb)	rmsd (m)	Radiosonde rmse (m)	Satellite rmse
10	113	30	109
30	72	22	69
50	74	18	72
70	68	16	66
100	69	14	68
200	55	10	54
300	43	8	42
400	43	6	43
500	44	5	44
700	34	3	34
850	26	2	26

rmsd between satellite and radiosonde geopotential heights to the geopotential height rmse for a single radiosonde and for the satellite. Little change in the rmsd occurs when the influence from the radiosonde is removed.

4.2.3 Winds

Geostrophic winds were computed from gradients of geopotential height taken from a hand analysis of the geopotential heights at each TOVS point. Since the dual radiosonde wind data were not processed, verifying radiosonde wind data were taken from radiosonde stations around Wallops Island, specifically, the 00Z soundings from Pittsburgh, Washington, D.C., and New York City. Fortunately, the NOAA-6 overpass times were no more than thirty minutes after these soundings were made.

A statistical comparison of the wind speed difference (satellite-radiosonde) is shown in Figure 4.8. Keep in mind that calculated geostrophic winds are compared to observed winds which are geostrophic only to a good approximation. Since this study has not formally addressed the precision of radiosonde winds, the rmsd is presented rather than the rmse attributed to the satellite alone. Figure 4.8 shows the rms wind speed difference to increase with height (decreasing pressure) from a minimum of 4 ms^{-1} at 850 mb to maximum values of 15 ms^{-1} at 100 mb. The magnitudes of these rms differences are comparable to those calculated by Carle and Scoggins (1981). It is known that the horizontal temperature gradient obtained from satellite mean layer temperatures tends to be smaller than the temperature gradient calculated from radiosonde temperature soundings (Phillips et al., 1979; Schlatter, 1981). The effect of this smaller gradient on the satellite-derived wind speeds can be seen in the shape
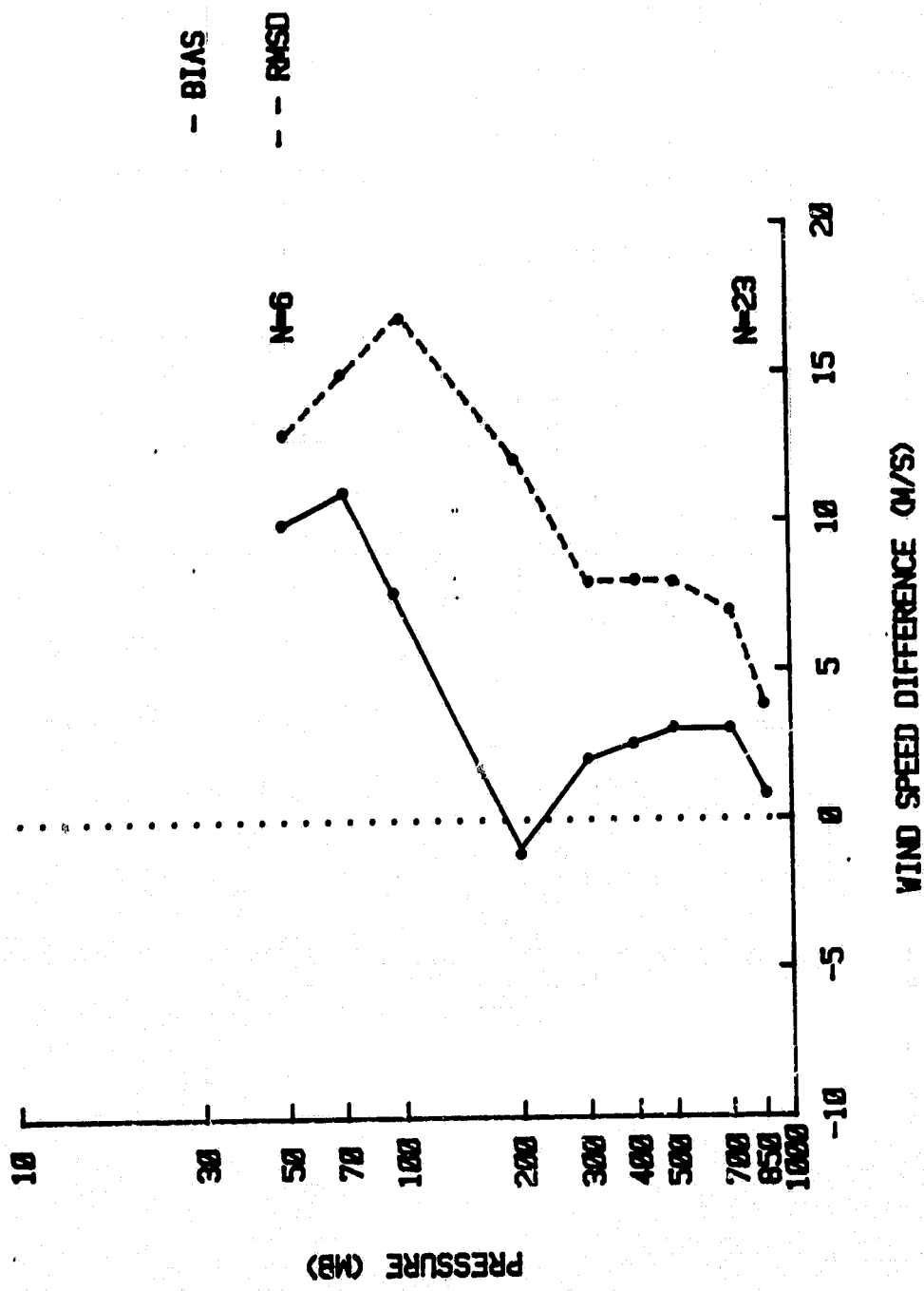
Figure 4.8 Average difference or bias (satellite-radiosonde) and
the root-mean-square difference for N comparisons
between satellite geostrophic wind speed and wind
speed determined by radiosonde.

of the bias curve in Figure 4.8. The bias decreases with height up to the approximate level of maximum winds ($\sim$ 200 mb). The radiosonde wind speeds are increasing with height faster than the satellite-derived wind speeds. Above the level of maximum winds, the bias becomes more positive with height, meaning the radiosonde wind speeds are decreasing more rapidly than the satellite-derived wind speeds. In each case, the satellite-derived winds have less vertical shear which implies a smaller horizontal temperature gradient.

A statistical comparison of the wind directions was also performed. The angle between the imaginary arrowheads of the satellite and radiosonde wind vectors was defined as the directional difference. Mean directional differences (satellite-radiosonde) and the rmsd are shown in Figure 4.9. The most notable curve is the rmsd. Throughout most of the troposphere and low stratosphere, values of 20° to 35° are seen. A rather distinct minimum of about 15° occurs at the approximate level of maximum tropospheric wind speed, a feature also seen by Carle and Scoggins (1981). Note also that the bias (mean difference) is nearly 0° at this level. Apparently, the direction of the geostrophic wind derived from satellite soundings better duplicates the observed wind direction under high wind speed conditions.

4.3 Satellite-Rocketsonde Comparisons

4.3.1 Mean Layer Temperature

Figures 4.10a and 4.10b show typical comparisons between satellite-derived temperature profiles interpolated to Wallops Island and single rocketsonde temperature profiles. As before, the
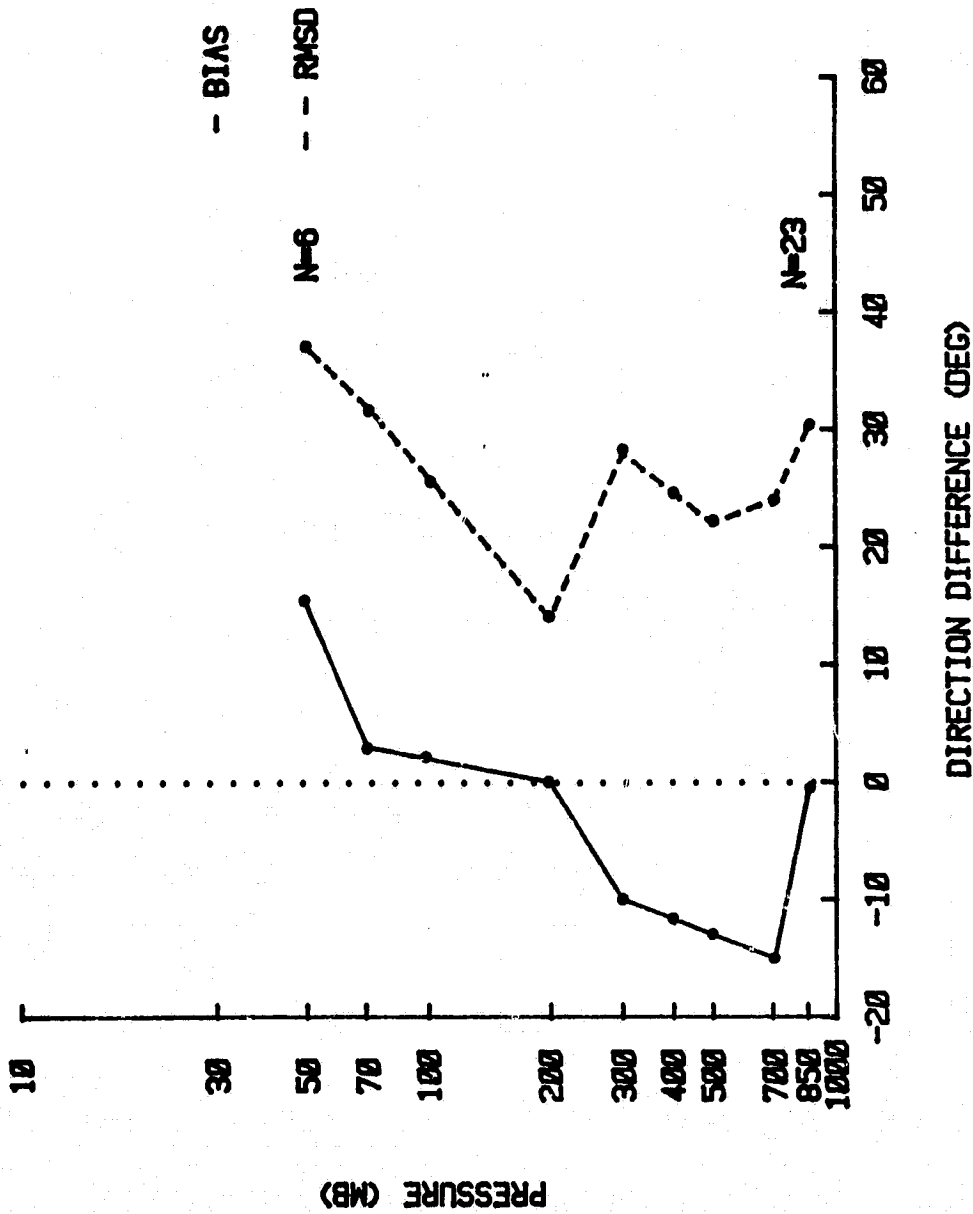
Figure 4.9 Average difference or bias (satellite-radiosonde) and the root-mean-square difference for N comparisons between satellite geostrophic wind direction and radiosonde wind direction.
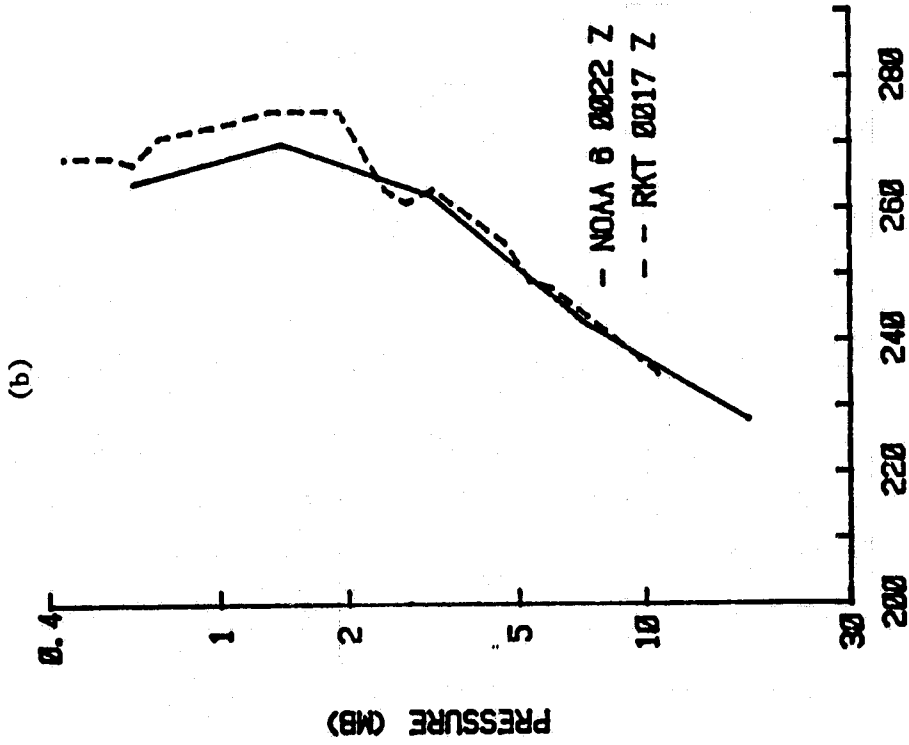
Figure 4.10b   Weighted-average satellite temperature profile and rocketsonde temperature profile of 16 May 1980.
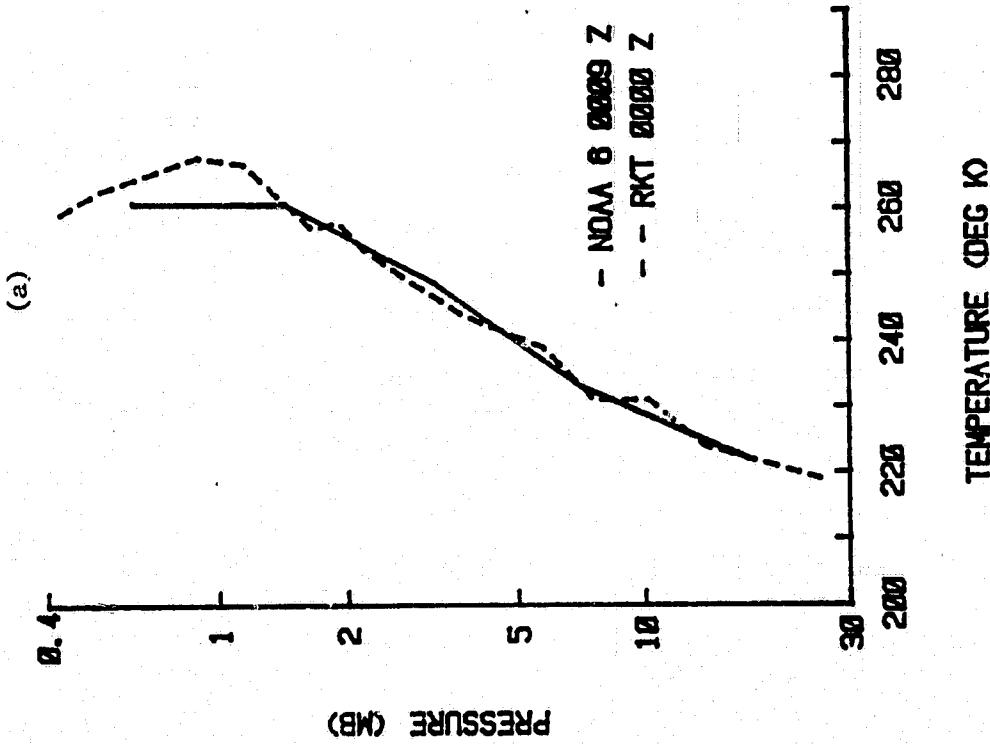
Figure 4.10a   Weighted-average satellite temperature profile and rocketsonde temperature profile of 10 April 1980.

satellite temperature profile was produced by plotting mean layer
temperatures at the center of each layer and by assuming a linear
temperature variation with decreasing pressure. Both figures show
reasonable agreement at and below about 2 mb, but above that level,
the rocketsonde temperatures are higher than those of the satellite.
Lack of vertical resolution is a major contributor to this character-
istic; the weighting function of the highest sensing channel of
NOAA-6 peaks at 2 mb. The satellite-derived temperatures underestimate
extreme temperature conditions. In these cases, the maximum in the
atmospheric temperature structure at stratopause levels is under-
estimated.

Figure 4.11 presents the summary of the statistical
comparisons between satellite-derived mean layer temperatures and
rocketsonde mean layer temperatures. The mean difference or bias,
ΔT, defined according to Equation 4.5 where $\overline{T}_I$ is now the rocketsonde
mean layer temperature, was calculated between the satellite and each
rocketsonde flown. Figure 4.11 shows the rocketsonde temperature to
be lower on average than the satellite by 1 K to 2 K, except in the
5-2 mb layer where the satellite mean layer temperature is, on
average, 1.5 K warmer. The reason for this anomaly is unknown.
Perhaps the appropriate NOAA-6 weighting functions needed adjustment
during the time of this study, or the anomaly could be a product of
the relatively small number (twenty-five successful rocketsonde flights)
of comparisons. It should be noted that in twenty of the twenty-five
comparisons for the 5-2 mb layer, the differences were greater
than 0 K, so the positive bias in this layer was consistently observed
and is not due to a small number of extremely large positive differences.

ORIGINAL PAGE IS
OF POOR QUALITY

TEMPERATURE DIFFERENCE (DEG K)

PRESSURE (MB)
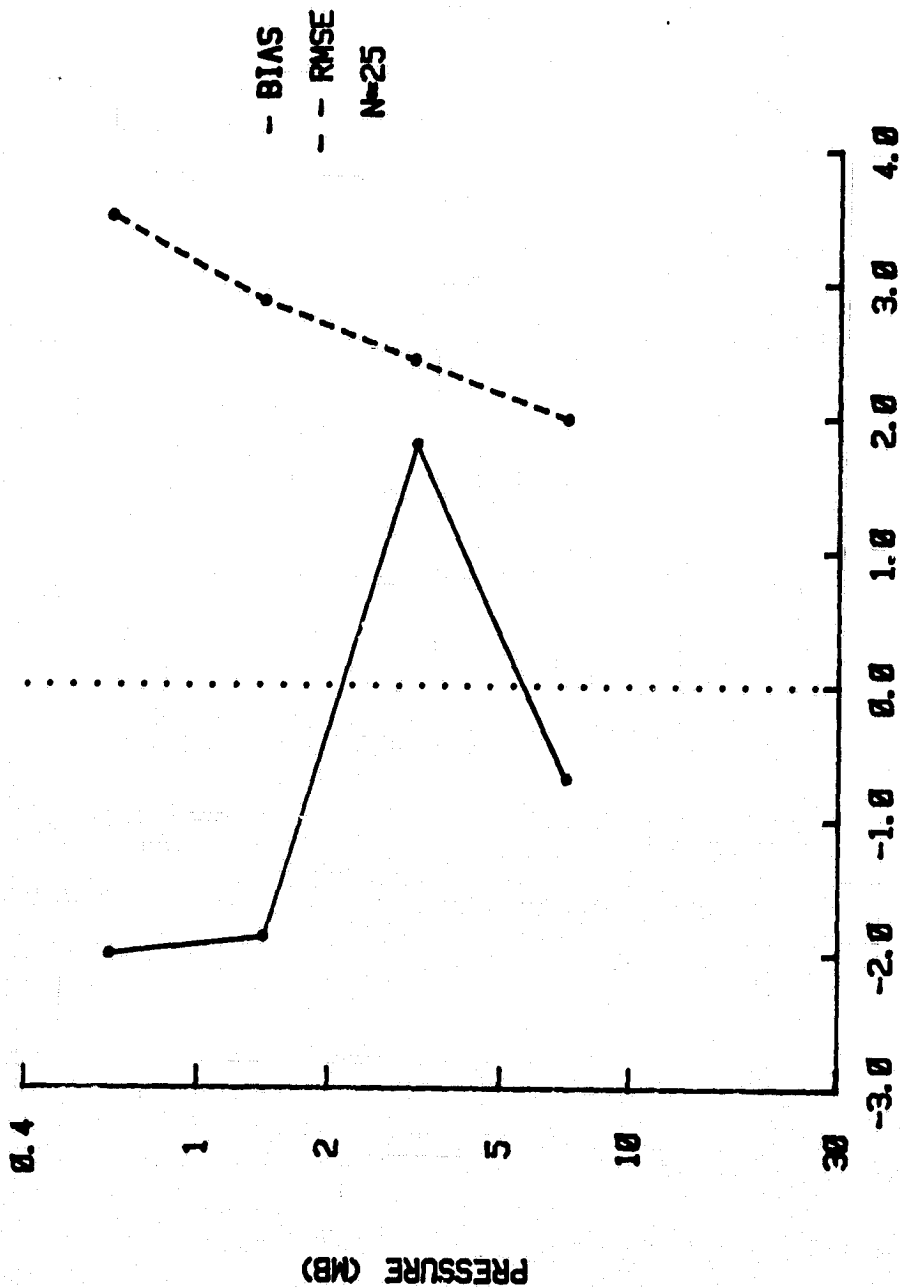
— BIAS
— — RMSE
N=25

Figure 4.11 Average difference or bias (satellite-radiosonde)
for N comparisons between satellite and rocketsonde
mean layer temperature, and the root-mean-square
error attributed to the satellite.

Figure 4.12 presents a histogram of the frequency of the 5-2 mb
mean layer temperature differences.

The rmse in the satellite mean layer temperature is shown as
the dashed line in Figure 4.11. The rmse increases with height to
3.5 K in the 1-0.4 mb layer, reflecting the loss of resolution
described above. Indeed, individual differences of up to -8 K were
observed in this layer. Six of the twenty-five comparisons had
differences between -4.5 K and -8 K. Six comparisons in the
2-1 mb layer had differences between -3.5 K and -6.5 K. Additional
work is required to produce satellite-derived mean layer temperatures
which are more comparable to rocketsonde temperatures at these high
levels.

Finally, it is again seen that the errors in the _in situ_ measure-
ments contribute little to the total variation between satellite mean
layer temperatures and _in situ_ mean layer temperatures. Table 4.5
shows the total rmsd between satellite and rocketsonde mean layer
temperatures and the mean layer temperature rmse for a single rocket-
sonde and for the satellite. Generally, most of the lack of agreement
between the two systems can be attributed to factors other than
imprecision in the rocketsonde temperatures.

4.3.2 Geopotential Height

Comparisons of geopotential heights are given in Figure 4.13.
Mean differences are no greater than 70 m at 0.4 mb, with rocketsonde
heights generally higher. The general shape of the bias in geopotential
heights reflects the bias in the mean layer temperatures. The
satellite rmse in geopotential height continually increases with
decreasing pressure to a value of 225 m at 0.4 mb. While the rmse
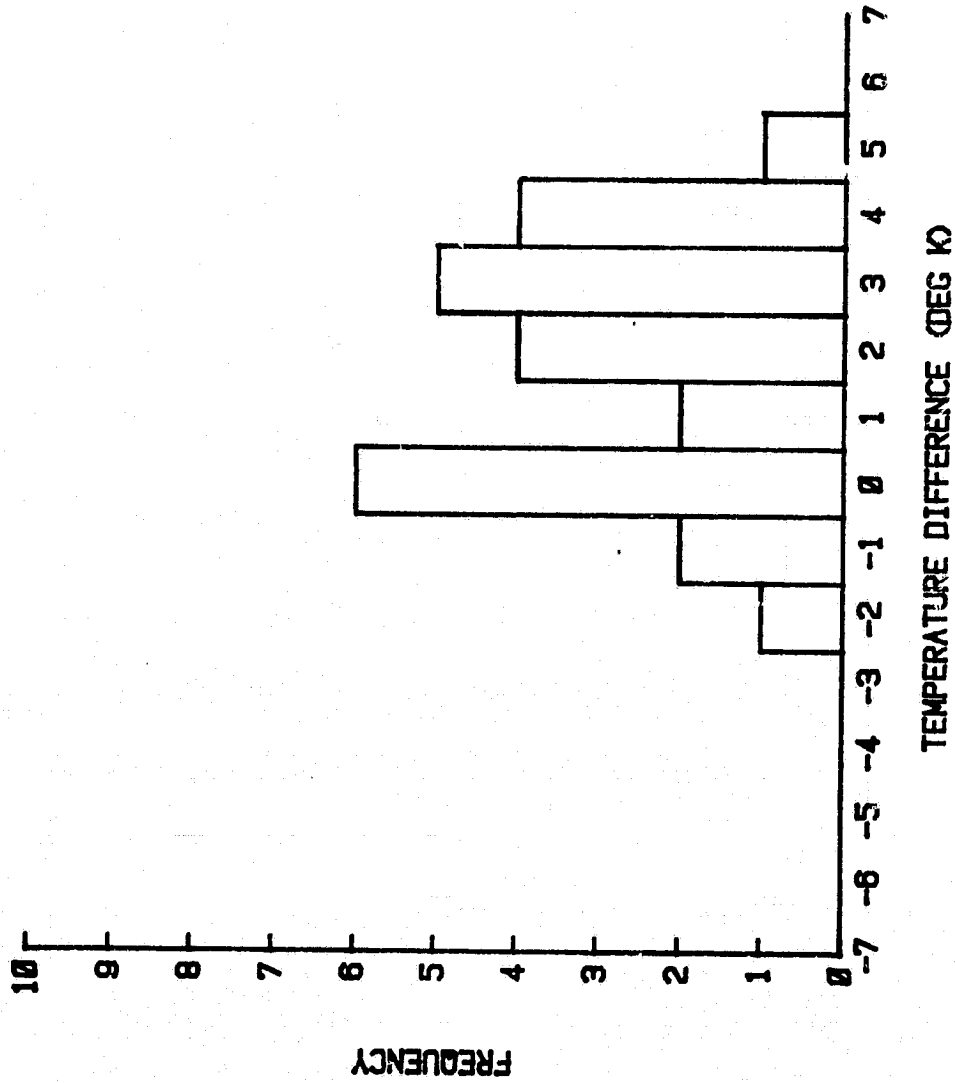
Figure 4.12 Histogram of the frequencies of mean layer temperature
differences between satellite and rocketsonde for the
5-2 mb layer.

ORIGINAL PAGE IS
OF POOR QUALITY
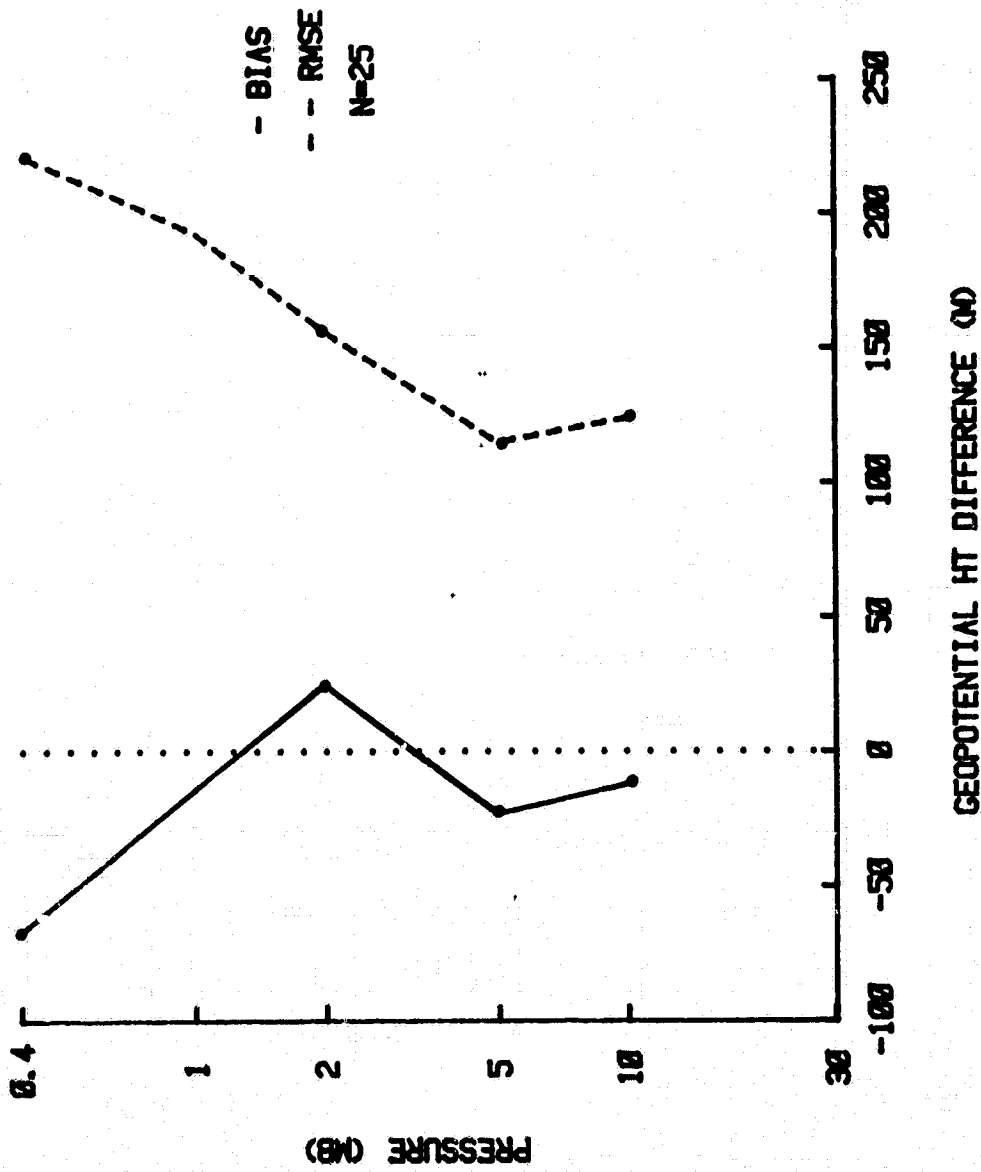
Figure 4.13 Average difference or bias (satellite-rocketsonde) for N comparisons between satellite and rocketsonde geopotential heights, and the root-mean-square error attributed to the satellite.

illustrates the decrease in the reliability of satellite-derived

geopotential heights with altitude, the magnitude of the rmse relative

to the height at which it is calculated is small.

Table 4.5   Comparison of root-mean-square differences (rmsd)
between satellite and rocketsonde mean layer
temperatures to the root-mean-square error (rmse)
in mean layer temperature for a single rocketsonde
and for the satellite.

Layer (mb)	rmsd (K)	Rocketsonde rmse (K)	Satellite rmse (K)
1-0.4	3.65	1.10	3.48
2-1	3.03	1.00	2.86
5-2	2.56	0.84	2.42
10-5	2.05	0.50	1.99

Table 4.6 presents the rmsd between geopotential heights of the

satellite and rocketsondes, the rmse in geopotential height for a

single rocketsonde, and the rmse in geopotential height attributed

to the satellite.   The rocketsonde rmse is rather high and is almost

comparable to the rmsd at some pressures.   The large rmse is due to

the tie-on problem.   Erroneous tie-on pressures lead to differences

in pressures calculated at any height between paired rocketsondes.

Because of these pressure differences, radar heights interpolated

to any pressure level can differ greatly among rocketsondes.   When

the rmse is subtracted out, the reduction in the rmsd ranges from

41 m (a 16% reduction) at 0.4 mb to 53 m (a 32% reduction) at the

5 mb level.   Percent reductions in the rmsd calculated for other

comparisons were much lower.   For example, when in situ errors

were taken into consideration, the largest reduction in the satellite-
rocketsonde mean layer temperature rmsd was 5.6%, while the satellite-
radiosonde rms geopotential height difference was reduced by at most
4%. Thus, due to the tie-on problem, errors in rocketsonde heights
had by far the largest impact on their respective comparison than
did any other in situ error.

Table 4.6   Comparison of root-mean-square differences (rmsd)
             between satellite-derived and rocketsonde geopotential
             heights to the root-mean-square error (rmse) in
             geopotential height for a single rocketsonde and
             for the satellite.

Pressure (mb)	rmsd (m)	Rocketsonde rmse (m)	Satellite rmse (m)
0.4	263	141	222
1	237	138	193
2	204	132	156
5	168	122	115
10	176	125	124

4.3.3 Winds

Hand analyses of the heights at each TOVS point provided height
fields from which geostrophic winds were calculated over Wallops
Island and compared to rocketsonde winds. Figure 4.14 presents the
bias (satellite-rocketsonde) and the rmsd of wind speed. The general
decrease of the bias with height again illustrates that the satellite-
derived geostrophic winds have less shear than the in situ winds.
The rmsd tends to increase with height to about 15 ms^{-1} at 0.4 mb.

Comparisons of the directional differences are given in Figure
4.15. The decrease with height of the rmsd from 65° at 10 mb to
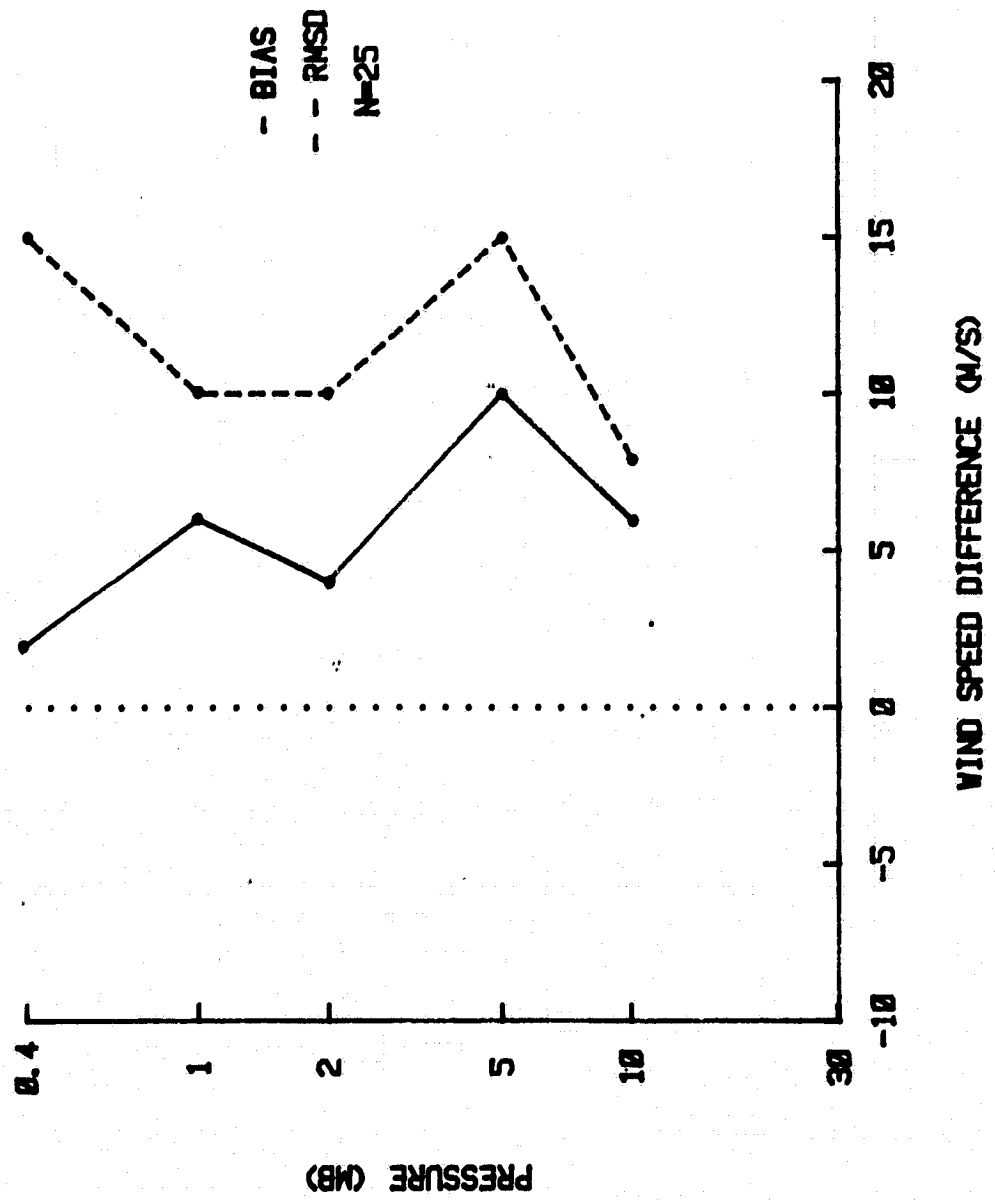
Figure 4.14 Average difference or bias (satellite-rocketsonde)
and the root-mean-square difference for N comparisons
between satellite geostrophic wind and wind speed
determined from rocketsonde.
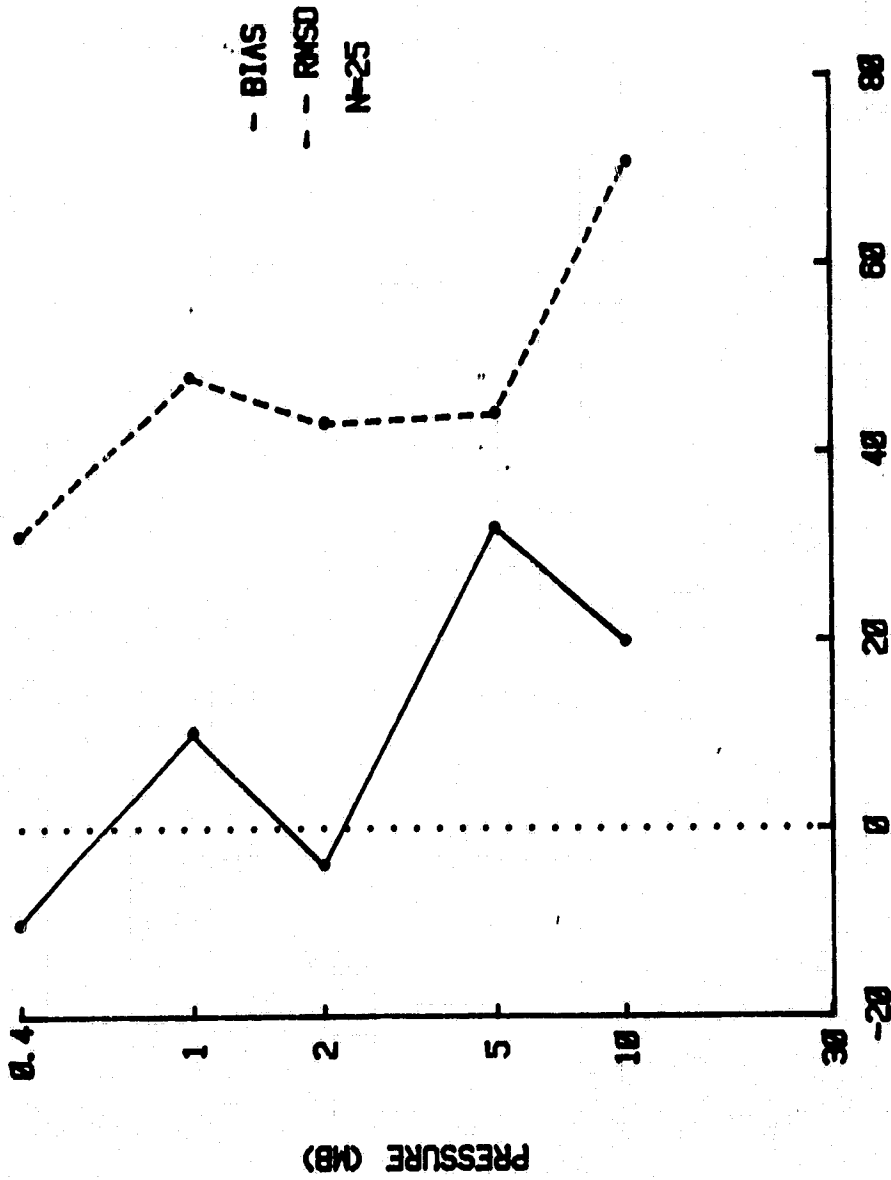
Figure 4.15 Average difference or bias (satellite-rocketsonde) and the root-mean-square difference for N comparisons between satellite geostrophic wind direction and rocketsonde wind direction.

25° at 0.4 mb is of interest. Figure 4.16 is a scatterplot of the absolute value of the directional differences versus the rocketsonde-determined wind speed. Note that there is a strong tendency for large directional differences to be associated with low rocket-sonde wind speeds. The majority of large differences are at the 10 mb level. Satellite-derived geostrophic wind directions tend to agree better with the rocketsonde wind directions under high wind speed conditions. Since winds are generally increasing with height in this part of the atmosphere, the rms direction differences decrease with height.
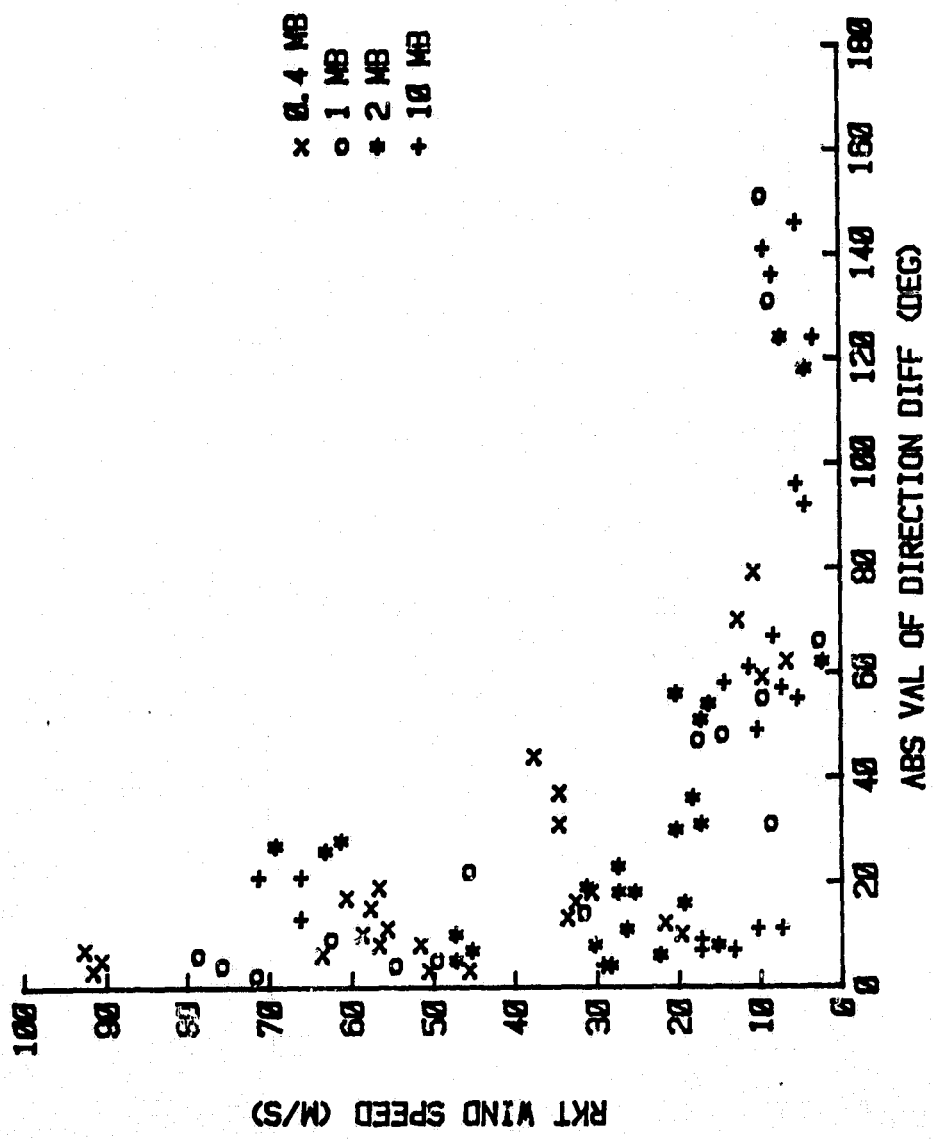
Figure 4.16 Scatterplot of the absolute value of the satellite-rocketsonde wind direction differences at various pressure levels as a function of rocketsonde wind speed.

C-2

5.0 SUMMARY, CONCLUSIONS, AND RECOMMENDATIONS FOR FUTURE WORK

Special flights of dual radiosondes and of meteorological rocket-sondes were made as close as possible in time to near overpasses of NOAA-6 above Wallops Island, Virginia. From those flights, the precision of _in situ_ measurements of layer mean temperature, geopotential height, and, for the rocketsondes only, winds, were evaluated. The dual radiosondes were also tracked by precision FPS-16 radar to evaluate geopotential height errors. Comparisons of the above quantities with those derived from NOAA-6 measurements were then performed with an emphasis on minimizing spatial and temporal variability between the satellite and _in situ_ measurements. The impact of _in situ_ measurement errors on the comparisons was also investigated.

Comparisons between dual radiosondes showed that the radiosonde provides precise pressure, temperature, and height information if the data are used as a function of radiosonde-measured pressure or of calculated height. Typical values of rms differences were 0.4-0.5 K, 0.3 mb, and 20 m for temperature, pressure, and geopotential height, respectively. It was concluded that the radiosonde provides precise data for synoptic-type purposes.

Tracking of the dual radiosondes with radar enabled the true measurement precision to be determined. Rms temperature differences calculated as a function of radar-determined height remained near 0.4 K, but rms pressure differences of 1-1.6 mb at tropospheric levels and up to 2 mb at stratospheric levels were found. This pressure imprecision was seen to cause large differences between

the true height of the radiosonde (as determined from radar) and
the height calculated with the hypsometric equation. It was suggested
that a radiosonde used in special "stand alone" work be tracked by
radar and the pressure profile be calculated in order to assign
the correct height to the balloon and to generate precise pressures.
Comparisons between the pressure-height profiles taken directly from
the dual radiosonde data and profiles computed with radar heights and
calculated pressures again showed that the radiosonde data does
estimate the correct pressure-height profile although the instrument
may never be located instantaneously at any point on that profile.

Studies of rocketsonde precision showed rms temperature differ-
ences to be 1-2 K up to about 55 km after which the rms differences
grew rapidly with height to almost 11 K. Rms geopotential height
differences ranged from 177 m at 10 mb to 199 m at 0.4 mb. Rms
differences computed for the wind components ranged from approximately
1 to 2 ms^{-1}.

Comparisons of layer mean temperatures from weighted-average
satellite soundings at Wallops Island to soundings from the in situ
instruments revealed that the largest rms errors attributed to the
satellite occur at the surface, in the tropopause region, and in the
uppermost layer (near the stratopause) sensed by the satellite. On
average, the satellite mean layer temperatures were higher than
those of the radiosondes near the surface and in the tropopause
region, and lower in the mid-troposphere. The satellite temperatures
were lower than those of the rocketsondes except in the 5-2 mb layer.
The effect of in situ temperature errors on these comparisons was
negligible.

The satellite rms error in geopotential height increased with height to 225 m at 0.4 mb. Overall, both the average differences and satellite rms error were small relative to the height at which they were calculated. Errors in the radiosonde heights had a negligible effect on the satellite-radiosonde height comparisons. Errors in the rocketsonde heights, however, had a rather large impact on the comparisons of satellite and rocketsonde heights.

Comparisons of geostrophic winds derived from a hand analysis of the satellite-derived heights to _in situ_ wind data showed the satellite-derived winds to have less vertical shear than winds determined from the _in situ_ instruments. There was also a tendency for the direction of the satellite-derived winds to better approximate the actual wind direction during times of high wind speed.

Based on this thesis, the following recommendations for future work are offered:

1. An explanation for the large variability in rocketsonde temperature measurements above 55 km is needed. Is this variability due to instrumental effects or does it reflect real atmospheric variability?

2. The continued development of satellite systems mandates that comparisons between these systems and _in situ_ systems be performed on a continual basis to evaluate the satellite data. To evaluate that data at stratospheric and mesospheric levels requires the use of rocketsondes, so it is important that rocketsonde launches continue.

3. Work is needed to improve the comparability of satellite temperatures to _in situ_ temperatures near the surface,

in the tropopause region, and in the stratopause region.
The development of a satellite with more than the twenty-
seven channels used today would increase the vertical
resolution of its temperature measurement and would allow
achievement of higher quality temperature soundings in the
regions mentioned above.

4. There is a continuing need for higher quality satellite
temperature soundings made under cloudy conditions. Improved
retrieval techniques and the development of an instrument
with added microwave channels would be welcomed.

5. A concentrated effort should be made to solve the "tie-on"
problem. What is the optimum way to choose an initial
pressure so that a pressure profile may be calculated
from rocketsonde data?

REFERENCES

Badgely, Franklin I., 1957: Response of radiosonde thermistors. Rev. Sci. Instr., 28, 1079-1084.

Ballard, H., and R. Rubio, 1968: Corrections to observed rocketsonde and balloonsonde temperatures. J. Appl. Meteor., 7, 919-928.

Bauer, Kenneth G., 1976: A comparison of cloud motion winds with coinciding radiosonde winds. Mon. Wea. Rev., 104, 922-931.

Bollerman, B., 1970: A Study of 30 km to 200 km Meteorological Rocket Sounding Systems. Contractor Report, NASA CR-1529, Marshall Space Flight Center, Huntsville, AL.

Broderick, H. J., C. Watkins, and A. Gruber, 1981: Statistical and Synoptic Evaluations of TIROS-N and NOAA-6 Retrievals. NOAA Technical Report NESS 86, Washington, D.C., 48 pp.

Bruce, R. E., L. D. Duncan, and J. H. Pierluissi, 1977: Experimental study of the relationship between radiosonde temperatures and satellite-derived temperatures. Mon. Wea. Rev., 105, 493-496.

Carle, William E., and James R. Scoggins, 1981: Determination of Wind from NIMBUS 6 Satellite Sounding Data. NASA RP 1072, Texas A&M Univ., College Station, TX. 72 pp.

Cressman, G. P., 1959: An operational objective analysis scheme. Mon. Wea. Rev., 87, 367-374.

Curtis, P. D., J. T. Houghton, G. D. Peskett, and C. D. Rodgers, 1974: Remote sounding of atmospheric temperature from satellites V. The pressure modulator radiometer for NIMBUS F. Proc. R. Soc. Lond., A 337, 135-150.

Danielsen, E. F., and R. T. Duquet, 1967: A comparison of FPS-16 and GMD-1 measurements and methods for processing wind data. J. Appl. Meteor., 6, 824-836.

Engler, N. A., J. K. Luers, J. W. McCloskey, and J. D. Strange, 1967: An Analysis of the AN/FPS-16 Rose System. Air Force Cambridge Research Laboratory Report AFCRL-67-0534, Air Force Cambridge Research Laboratories, Office of Aerospace Research, U.S. Air Force.

Finger, F. G., M. E. Gelman, F. J. Schmidlin, R. Leviton, and B. W. Kennedy, 1975: Compatibility of meteorological rocketsonde data as indicated by international comparison tests. J. Atmos. Sci., 32, 1705-1714.

_____, and R. M. McInturff, 1978: The Compatibility of Upper Air Data, Part I: Research on Compatibility of Data from Radiosondes, Rocketsondes, and Satellites. World Meteorological Organization Technical Note 163, Geneva, Switzerland, 103 pp.

Godson, W. L., 1963: The representation and analyses of vertical distributions of ozone. Quart. J. Roy. Meteor. Soc., 89, 220-232.

Grubbs, F. E., 1948: On estimating precision of measuring instruments and product variability. J. Amer. Stat. Assoc., 43, 243-264.

Hodge, M. W., and C. Harmantas, 1965: Compatibility of United States radiosondes. Mon. Wea. Rev., 93, 253-266.

Hoehne, Walter E., 1980: Precision of National Weather Service Upper Air Measurements. NOAA Technical Memorandum NWS T&ED-16, Sterling, VA, 23 pp.

Iribarne, J. V., and W. L. Godson, 1973: Atmospheric Thermodynamics. D. Reidel Publishing Co., 259 pp.

Jastrow, R., and M. Halem, 1973: Accuracy and coverage of temperature data derived from the IR radiometer on the NOAA 2 satellite. J. Atmos. Sci., 30, 958-964.

Kaplan, L. D., 1959: Inference of atmospheric structure from remote radiation measurements. J. Opt. Soc. Amer., 49, 1004-1007.

Kennedy, J. S., and W. Nordberg, 1967: Circulation features of the stratosphere derived from radiometric temperature measurements with the TIROS-7 satellite. J. Atmos. Sci., 24, 711-719.

King, J. I. F., 1956: The radiative heat transfer of Planet Earth. In Scientific Uses of Earth Satellites. Univ. of Michigan Press, Ann Arbor, Mich., 133-136.

Krumins, M. V., 1976: Measurement of Air Temperature at High Altitudes by Rocketsonde Immersion Thermometry Technique. Ph.D. Dissertation, University of Maryland, College Park, Maryland.

Lenhard, Robert W., 1970: Accuracy of radiosonde temperature and pressure-height determination. Bull. Amer. Meteor. Soc., 51, 842-846.

_____, 1973: A revised assessment of radiosonde accuracy. Bull. Amer. Meteor. Soc., 54, 691-693.

Luers, J. K., and C. D. MacArthur, 1971: Optimum Radar and Filters for the Passive Sphere System. NASA Contractor Report CR-111952.

McInturff, R. M., F. G. Finger, K. W. Johnson, and J. D. Laver, 1979: Day-Night Differences in Radiosonde Observations of the Stratosphere and Troposphere. NOAA Technical Memorandum NWS NMC 63, U.S. Dept. of Commerce, Washington, D.C., 47 pp.

Middleton, W. E. Knowles, 1969: Invention of the Meteorological Instruments. Baltimore: The Johns Hopkins Press, 362 pp.

Miller, A. J., and F. J. Schmidlin, 1971: Rocketsonde repeatability and stratospheric variability. J. Appl. Meteor., 10, 320-327.

Moyer, V., J. R. Scoggins, Nine-Min Chou, and G. S. Wilson, 1976: Atmospheric structure deduced from routine NIMBUS 6 satellite data. Mon. Wea. Rev., 106, 1340-1352.

Phillips, N. A., L. M. McMillin, A. Gruber, and D. Q. Wark, 1979: An evaluation of early operational temperature soundings from TIROS-N. Bull. Amer. Meteor. Soc., 60, 1188-1197.

_____, 1980: Two examples of satellite temperature retrievals in the north Pacific. Bull. Amer. Meceor. Soc., 61, 712-717.

Phillips, P. D., H. Richman, J. Joss, and A. Ohmura, 1981: ASOND-78: An intercomparison of Vaisala, VIZ, and Swiss radiosondes. Pure Appl. Geophys., 119, 259-277.

Rapp, R. Robert, 1952: The effect of variability and instrumental error on measurements in the free atmosphere. New York University College of Engineering Meteorological Papers, 2, 1-41.

Schlatter, T. W., 1981: An assessment of operational TIROS-N temperature retrievals over the United States. Mon. Wea. Rev., 109, 110-119.

Schmidlin, F. J., 1981: Repeatability and measurement uncertainty of the United States meteorological rocketsonde. J. Geophys. Res., 86, 9599-9603.

Schwalb, Arthur, 1978: The TIROS-N/NOAA A-G Satellite Series. NOAA Technical Memorandum NESS 95, Washington, D.C., 75 pp.

Smith, W. L., and H. M. Woolf, 1976: The use of eigenvectors of statistical covariance matrices for interpreting satellite sounding radiometer observations. J. Atmos. Sci., 33, 1127-1140.

_____, C. M. Hayden, D. Q. Wark, and L. M. McMillin, 1979: The TIROS-N operational vertical sounder. Bull. Amer. Meteor. Soc., 60, 1177-1187.

Wang, Jen-yu, 1975: Instruments for Physical Environmental Measures, Vol. 1. Milieu Information Service, 386 pp.

Wark, D. Q., and D. T. Hilleary, 1969: Atmospheric temperature: Successful test of remote probing. _Science_, _165_, 1256-1258.